Chair of Ferrous Metallurgy

Master's Thesis

OPTIMIZATION OF HEAT TRANSFER MODEL USED IN THE CONTINUOUS CASTING OF STAINLESS STEEL

Muhammad Wahib

March 2024

MONTANUNIVERSITÄT LEOBEN
www.unileoben.ac.at

AFFIDAVIT

I declare on oath that I wrote this thesis independently, did not use any sources and aids other than those specified, have fully and truthfully reported the use of generative methods and models of artificial intelligence, and did not otherwise use any other unauthorized aids.

I declare that I have read, understood and complied with the "Good Scientific Practice" of the Montanuniversität Leoben.

Furthermore, I declare that the electronic and printed versions of the submitted thesis are identical in form and content.

Date 04.03.2024

Signature Author
Muhammad Wahib

KU LEUVEN

FACULTEIT
INGENIEURSWETENSCHAPPEN

OPTIMIZATION OF HEAT TRANSFER MODEL USED IN THE CONTINUOUS CASTING OF STAINLESS STEEL

Muhammad Wahib

Thesis submitted to obtain the degree
of Master of Materials Engineering

Thesis supervisor:
prof. dr. ir. Bart Blanpain
dr. ir. Shuigen Huang
dr. ir. Annelies Malfliet

Assessor:
prof. dr.ir. Christian Bernhard
prof. dr. ir. Yentl Swolfs

Mentors:
ir. Mohammad Khoshahang
ir. Yijie Liang
ir. Bastien Soete
ir. Anna Roca Sanchez

Academic year 2023-2024

Forward

As I get closer to finishing my master's degree, I am thankful to the people who have guided and supported me throughout my master thesis.

First, I extend my deepest appreciation to my esteemed supervisors, prof. dr. ir. Bart Blanpain, dr. ir. Shuigen Huang and dr. ir. Annelies Malfliet. Their expertise, patience, and unwavering support have been crucial throughout the thesis process. I am particularly grateful for the continuous guidance and insightful feedback in refining my research.

My heartfelt gratitude also goes to my daily supervisors at KU Leuven, ir. Mohammad Khoshahang and ir. Yijie Liang, who were always there to guide me throughout the thesis and to give valuable suggestion. Mohammad, thank you from the start of the thesis, with the CFD training to the throughout support, guidance, and trust. Yijie, thankyou from the start, assistance with the calculation of thermophysical parameters, and the continuous guidance throughout the thesis.

At Aperam, I am immensely grateful to my supervisor, ir. Anna Roca Sanchez. Her support and the provision of necessary facilities within Aperam have been essential in enabling me to conduct simulations on Aperam's cooling system. I am grateful for providing every detail in supporting the findings of my thesis and specially the pyrometer data for the validation.

I want to thank prof. dr. ir. Christan Bernhard from MU Leoben, Austria for providing the IDS thermophysical parameters data for steel grades that made a significant contribution in the completion of the thesis. I am truly grateful for his assistance and knowledge in this area of research.

Finally, I cannot express in words the thankfulness I have for my family and friends, who have been my strength and support throughout my academic journey. Their love, motivation, and faith in my abilities have motivated me through the challenges and setbacks. I am eternally grateful for their sacrifices and continuous support.

This thesis is a major step forward in my learning, and I am deeply thankful to all those who have played a part in this journey. Their contributions have shaped my understanding of research and have instilled in me a passion for lifelong learning. I am committed to carrying forward their legacy of excellence and making a positive impact on the world through my research endeavours.

Table of Contents

Abstract

The continuous casting process is a crucial step-in stainless-steel production that involves the solidification of molten steel into continuous slabs or blooms. This casting process involves transferring of molten steel from a tundish to a water-cooled mold, where solidification starts. As the solidifying strand exits the mold, it is supported by rotating rollers in the secondary cooling zone. Water and air mist is continuously sprayed to achieve complete solidification. After complete solidification, the slabs are cut and sent for further processing.

The efficient control of heat transfer is crucial to optimize the casting process, preventing casting defects and enhancing production efficiency. A key challenge in continuous casting is preventing breakout of the liquid metal, which occurs when the solid shell is too thin, leading to rupture and spilling of liquid metal. The shell thickness depends on the heat transfer behaviour during solidification.

This thesis is performed in collaboration with the stainless-steel company Aperam and focuses on optimizing the heat transfer model used in continuous casting of stainless steel. The heat transfer model is influenced by the thermodynamic properties of steel including heat capacities, solidification enthalpy, and heat transfer coefficients. The primary objective is to provide Aperam with accurate thermodynamic inputs for steel grade 304L and 316L, enabling a thorough understanding of the model's dependence on these values. For this Thermo-Calc and IDS databases are used to collect different thermophysical parameters. Additionally, a CFD heat transfer and solidification model is developed considering the Aperam continuous casting plant conditions, and respective heat transfer coefficients (HTCs) are calculated for the mold and the secondary cooling region. These inputs are used to predict the temperature and solidification profiles at different sets of casting speeds and superheat values for both steel grades in the DYNACS and CFD model. Further these models' temperature results are compared with the real temperature data acquired from a pyrometer at the continuous caster.

The findings of this study highlighted the importance of accurate thermophysical parameters and heat transfer conditions. Further, the parametric study investigated the role of individual thermophysical parameters on the temperature and solidification profiles and helped to predict the behaviour of steel grades under varying process conditions such as casting speeds and superheat values.

This study provides Aperam a valuable insight into the relationship between the thermophysical parameters and solidification profiles. This knowledge will enable the company to optimize the process conditions, such as casting speed, maximizing the production efficiency, and minimizing the risk of breakout defects.

List of figures and tables

List of figures

List of tables

List of abbreviations and symbols

Abbreviations

AOD	Argon Oxygen Decarburization
CFD	Computational Fluid Dynamics
CALPHAD	Calculation Of Phase Diagrams
DRI	Direct Reduced Iron
DYN3D	Dynamic Three-Dimensional Model
EAF	Electric Arc Furnace
FP	Ferrite Potential
FEM	Finite Element Method
FVM	Finite Volume Method
HBI	Hot Briquetted Iron
HTC	Heat transfer coefficient
IHTP	Inverse Heat Transfer Problem Model
IDS	Inter - Dendritic Solidification
ML	Metallurgical Length
SEN	Submerged Entry Nozzle
SCR	Secondary cooling region
SS	Stainless Steel

Symbols

γ	Austenite
δ	Ferrite
c(T)	Leidenfrost effect
D_p	Diameter of droplet
N	Droplet number density
Q	Heat flux
v_o	Impingement velocity
$Cr_{eq.}$	Chromium equivalent
$Ni_{eq.}$	Nickel equivalent
T_{SA}	Solidification temperature
avCS(i,t)	Average casting speed at loop 'i' and time 't'
sh(x,t)	Shell thickness at position x and time t
t_{strand}	Time spent by steel in the strand
T_{surf}	Surface temperature
$T_{ambientM}$	Ambient temperature for mold
$T_{ambientR}$	Ambient temperature for the radiation
$T_{ambientW}$	Ambient temperature for the water flow
T_{ext}	External temperature
T_s	Surface temperature
K	Solidification factor for the mold and the secondary cooling region
ε	Emissivity
C_p	Specific heat
$C_{p.eff}$	Effective specific heat capacity
$K_{eff.}$	Effective conductivity
Q_L	Source term
H_{ref}	Reference enthalpy
h	Sensible heat
L	Latent heat of material
β	Liquid fraction
$\bar{u}_{pull}$	Pull velocity
$\mu_{eff.}$	Effective viscosity
μ_l	Dynamic viscosity
μ_t	Turbulent viscosity
A_{mush}	Mushy zone parameter
S	Momentum sink
ρ_ω	Density of water
C_ω	Specific heat of water
k_w	Thermal conductivity of cooling water
Re_w	Reynold number of cooling water
Pr_w	Prandtl number of cooling water
D_H	Hydraulic diameter
$\lambda_{eff.}$	Effective thermal conductivity
∇	Nabla operator

Γ	Diffusion coefficient
q_m	Heat flux of mold
V_{cast}	Casting speed
A_{roller}	Contact surface area of rollers
L_m	Mold length
W_L	Water flow rate in mold
ω	Spray cooling flux
α	Machine dependent calibration factor

Chapter 1: Introduction

1.1 Project Framework

Continuous casting (CC) is a highly prevalent technique for steel production with the annual production of more than 1.2 billion tons of steel. The produced steels are in semi-finished and finished shapes. To meet the growing demand of high-performance steels, the primary focus is to augment the production efficiency and minimize production cost for the steels produced by continuous casting. Steel producers encounter a range of difficulties in manufacturing high quality steels. To achieve these goals, better technologies are being introduced and existing products are being optimized by extensive research on improving the final quality and production efficiency.

The continuous casting process begins with the preparation of steel melt in an AOD furnace, where the steel's chemical composition is meticulously controlled to meet the precise requirements for the desired product. The ladle is used to transfer the molten steel from the AOD furnace to the tundish. The tundish is a large container that provides a stable environment and allows for it to be distributed evenly into the mold. The molten steel passes through the submerged entry nozzle (SEN) at a controlled rate into the open-ended copper mold. There is a layer of mold flux, which is usually oxide or liquid oxide melt on the mold surface to avoid the contact of molten steel with the mold walls. Mold flux has a large impact on the casting behavior, such as reducing oxidation, minimizing heat loss, and enhancing surface quality. Liquid steel starts to solidify in the mold region, and the solidifying strand slides on the support roller to the secondary cooling region, where solidification is completed. Primary and secondary cooling regions are used to solidify the steel by extracting the heat from the solidifying steel. The primary cooling region consists of water channels at different parts of the copper mold. The secondary cooling region consists of high-pressure spray nozzles at the secondary cooling regions. The solid shell formation starts at the mold walls and the cast steel is drawn at the given casting speed. After complete solidification, the steel is moved to the cutting station [1].

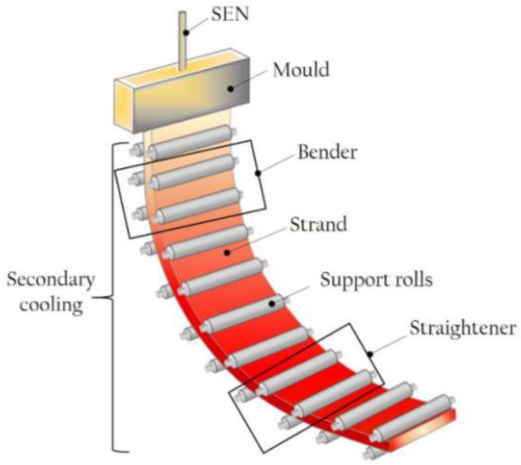

Figure 1: A simplified illustration showcasing the continuous solidification of molten steel into a solid strand

In recent decades, many developments have been done to increase the production efficiency. A wide range of mold flux powders and improvement of oscillation settings have been used to minimize the friction forces between the moving solidifying steel and water-cooled mold walls. There has been considerable improvement in controlling various casting defects that are attributed to the interplay between steel grade, mold flux and different casting conditions. It is necessary to optimize the casting speed and water spray rate to solidify the steel properly and to minimize casting defects. There can be various reasons by which the casting speed can change during the casting, among which the breakout detection alarm, ladle changes and delay in the operating time during the casting of the caster. It is very important to keep the surface temperature under control as it is the main reason for the crack initiation. A proper temperature distribution in the overall casting process is necessary which can be controlled by water spraying [2].

Numerical modelling is very helpful in solving complex engineering problems in the continuous casting process to save time and operating costs in the industrial sector. For the past few decades, there has been a substantial improvement in computational fluid dynamics codes. By coupling different physical models, many complex processes can be simulated by CFD modelling. To investigate the heat transfer, fluid flow and solidification processes during the continuous casting, which involves a multitude of intricate physical phenomena, poses a significant challenge for computational modelling. The methodology adopted by computational fluid dynamics (CFD) measurements closely aligns with the real-world applications, such as the temperature profiles obtained from thermocouples.

1.2 Problem statement

Aperam is a producer of stainless, electrical and specialty steels which operates in Europe and South America with main production facilities in Belgium, France, and Brazil.

It offers a wide variety of different steel grades and alloys which have applications in different industrial and private sectors.

The Aperam Genk plant is a stainless-steel melting and finishing site. It is recognized as a reference for sustainable development. The steel scrap and other primary units (DRI, HBI, etc.) are melted in an Electric Arc Furnace (EAF), with a production capacity of 1 million tons per annum [3].

In the next step, the elemental composition is precisely adjusted in an Argon Oxygen Decarburization (AOD) furnace and then the molten steel is charged into the ladles, where final composition is achieved through the addition of the last raw materials, and then it is poured into the tundish for the continuous casting process. The solidification of steel initiates in the mold region and continues along the caster segments, where it undergoes a controlled cooling process using water-mist sprays, until reaching full solidification. The solidified steel strand is cut into slabs of weight up to 30 tons, up to 12 m in length, thickness of 200 mm and up to 2 m wide. It is moved further to the hot rolling step and then moved to the annealing and cold rolling line depending on the desired properties. In the last stages, the desired shapes are finished in the finishing shop prior to transportation.

For continuous casting, Aperam uses a heat transfer model to simulate the heat transfer and solidification behavior. During the casting of stainless steels, it is necessary to control the casting speed and the water-flow rate to prevent the breakout of the liquid metal, which is a major issue for the safety and for the condition of the caster. Breakout may occur when the solid shell is too thin beneath the mold, which results in the shell cracking and subsequent spilling out of liquid metal. The steel shell thickness is related to the management of the heat transfer in the mold and in the spraying chamber. The controlled casting speed and cooling rate is important to avoid the breakout of liquid metal as well as impacting the final quality of cast product. Aperam requires insight in the dependency of the solidification behavior on the specific steel grade through using thermophysical properties. A computational model could in addition provide a validation of the current heat transfer model. The outcome will provide useful insight in the dependency of the solidification behavior on the steel grade and will allow to optimize the casting speed and production efficiency without having the risk of breakout.

Chapter 2: Literature review

2.1 Developments in continuous casting

In the middle of the 19th century (1843), twin roll casting was developed as a continuous casting process for copper and its alloys. In 1856, Henry Bessemer applied and patented this process for the casting of steels [4]. With the advancement of technology, various modifications have been made to make it more effective and precise and to optimize the steel quality. Since the 1950's, continuous casting has therefore been an area of attraction for the steel producers as an alternative to the ingot casting process. It can produce near net shape castings with lower operating costs. The production and use of continuous casting in the steel industry started to increase in the late 19th century as the worldwide petroleum and energy crisis in 1973 forced the major steel producers to make developments in their continuous casting processes to compete in the market and avoid an economic recession. Since then, continuous casting plants have been restructured and reconstructed majorly focusing on moving toward automatic and controlled processing to save manpower, reducing the cost and to maximize the output and quality of the final casting. Focusing on these goals, continuous casting has become the chosen and effective way for the production of crude steel, whereas ingot casting processes can only be used nowadays for unique process applications [5].

2.1.1 Basics of continuous casting process

The continuous casting process involves a physical phenomenon of continuously solidifying the liquid steel into a strand to produce a variety of different shapes depending on the cross-section area such as bloom, slabs, and billets. Steel production starts with the production of crude steel for which there are two predominant routes [Figure 2] [6]:

- **Smelting process**: Iron ore is crushed into fine particles and agglomerated along with flux fine by using coke fines as solid fuel in a sintering plant. Then this sintered iron ore and coke is filled in the blast furnace. The combustion process of coke occurs by blowing the hot air (1200 °C) from the inlet tuyeres in the blast furnace. The carbon monoxide formed in earlier step reduces the iron oxides. Besides, the molten mixture of iron, called *pig iron,* is removed from the bottom with a slag. Pig iron settles down and the slag floats on it due to the lesser density of the slag. This pig iron is approximately at 1400 °C and is poured onto the scrap bed in a giant oxygen converter which then heats it to 1600 °C in the presence of oxygen for removing the unwanted impurities such as C. The obtained molten liquid is called crude steel.
- **Electric melting process:** In this process, scrap and other primary units, such as Direct Reduced Iron (DRI) and Hot Briquetted Iron (HBI), are melted in a large electric furnace. Electrodes are present in the electric furnace, which generate a powerful arc and melts the solid scrap into liquid crude steel.

This crude steel is then fed into the refining unit, where carbon content is adjusted along with other alloying elements. The temperature is under control between the refining and the casting.

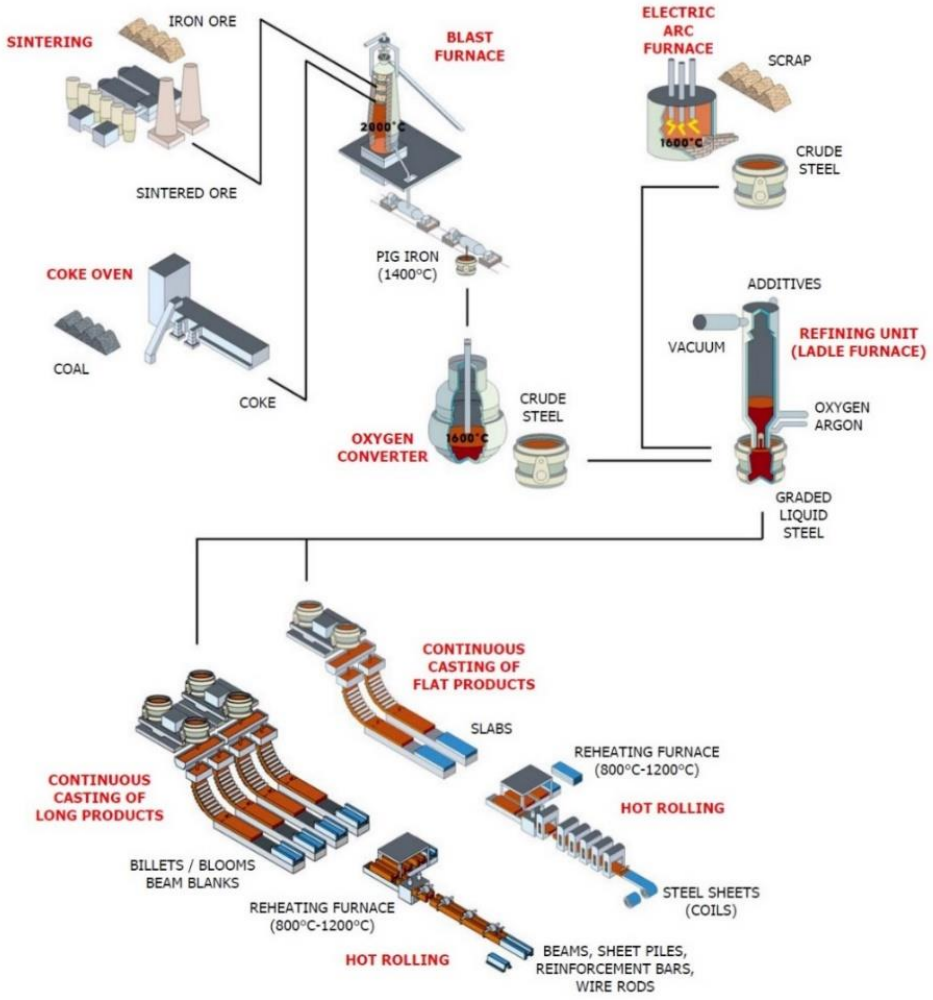

Figure 2: Process flow of steelmaking process [7].

The molten steel from the refining unit comes to the continuous casting unit by successive ladles. To provide a continuous flow of melt to the caster, the steel from the ladles is poured in the tundish. The tundish has a hole at the bottom from where the liquid melt flows to the mold. The tub shaped design of the tundish helps the removal of inclusions as the inclusions gather at the top layer of slag which is further removed from the melt surface. This slag removal is necessary to avoid surface defects in the final casting. The remaining inclusions inside the melt from the tundish can cause surface cracks such as ‘slivers’ in the rolling step. Large inclusions can result in a lower strength and resistance to fatigue of the steel. For higher quality steel, the slag layer must be protected from air to avoid the formation of detrimental oxide inclusions [8].

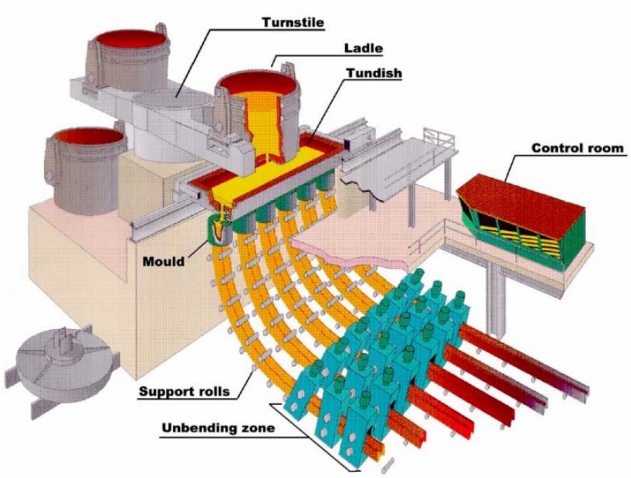

Figure 3: Continuous casting mill [7].

The liquid steel in the tundish flows through the ceramic nozzle called submerged entry nozzle (SEN) into the mold [Figure 3]. The liquid melt starts solidifying in the water - cooled copper walls. The mold oscillates in the vertical direction to avoid the prevent the shell from adhering to the mold walls. The casting speed is primarily adjusted according to the cooling profile and the required shell thickness based on the specific steel grades .The solidifying shell is drawn out from the mold by using water – cooled rollers. The liquid flow rate depends on the nozzle opening and it is controlled from the mold level sensors. As the solidifying shell enters the mold region, the mold flux layer provides a protective layer against oxidation, reducing heat loss, and promoting proper meniscus formation [Figure 4] which contributes to the overall casting quality. The mold flux layer generates the thermal insulation and help in a steady heat flow for the casting and helps in avoiding the inclusions in the meniscus region [9].

The temperature of the bottomless mold is usually kept at 100 – 200 °C, so when liquid melt hits the walls of the cooled mold, it freezes, and solidification starts. The partially solidified steel is entered into the secondary cooling region where water and air is continuously sprayed in between the support rolls to cool the strand surface. The distance from the liquid melt in the mold region to the point where solidification is completed is called as metallurgical length (ML). After this point, the casted strands are cut down in the desired lengths for further rolling and finishing processes.

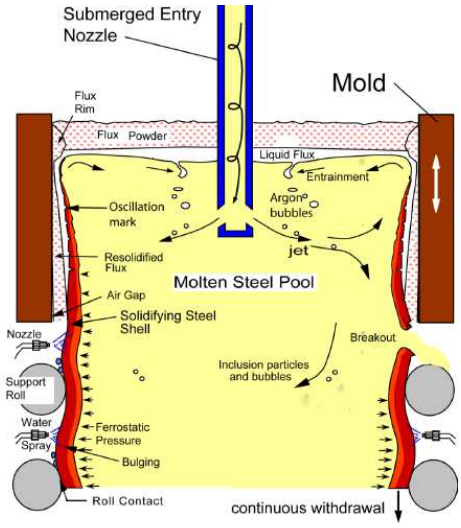

Figure 4: Schematic illustration of steel flowing from SEN into the mold region[10].

2.1.2 Advancement of continuous casting machine designs

Continuous casting machines were developed on vertical casting machine designs. The support rollers in vertical continuous casting process bears very high stresses due to the ferro - static forces acting on the strand. In 1965, considering the drawbacks of vertical continuous casting, the machine design was changed from totally vertical to the curved continuous caster [Figure 5 (a)]. Nowadays, the curved mold with straightening machine is usually used for casting operations. The curved continuous casting is beneficial in terms of reducing the operational cost and maintenance issues. Also, the strand quality is highly improved by using the curved continuous caster. With years, the use of the curved caster is increased for slab and bloom - billet casters as compared to other casting designs [Figure 5(b)] [11].

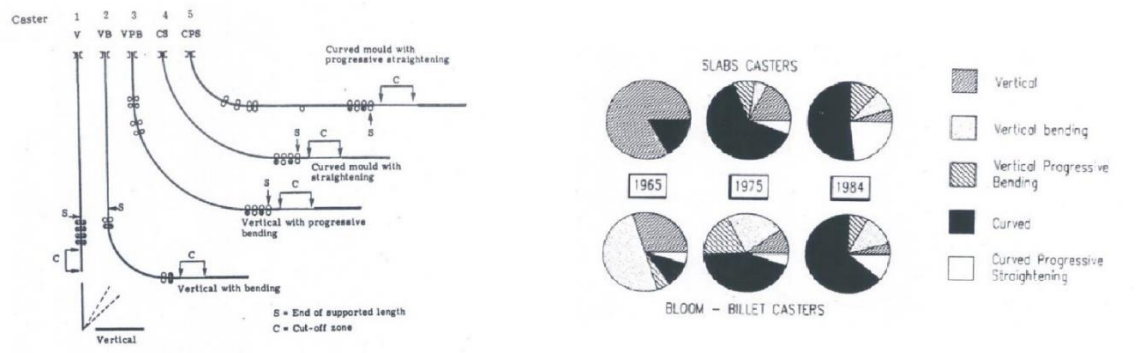

Figure 5: (a) Types of Continuous casting machine designs. (b) Global demand for different continuous casting machine designs for slab, bloom and billets casters [11].

The strand with progressive straightening can be used for the casters of larger heights. In progress of decreasing the height of the mold, the horizontal continuous casting machine was also used, but it has problems such as the difficulty to cast strands with large cross-section area, issues with the separation of the solidified shell from the mold

and low stability. Operational horizontal continuous casting machines are nowadays limited to billet casting [12].

In curved continuous casting, bending and straightening operations are introduced in the solidifying steel. As bending imposes longitudinal tensile stresses on the outer curve and compressive stresses on the inner curve while going from bending to straightening, it imposes a compressive stress on the outer curve and a tensile stress on the inner curve [Figure 6][13].

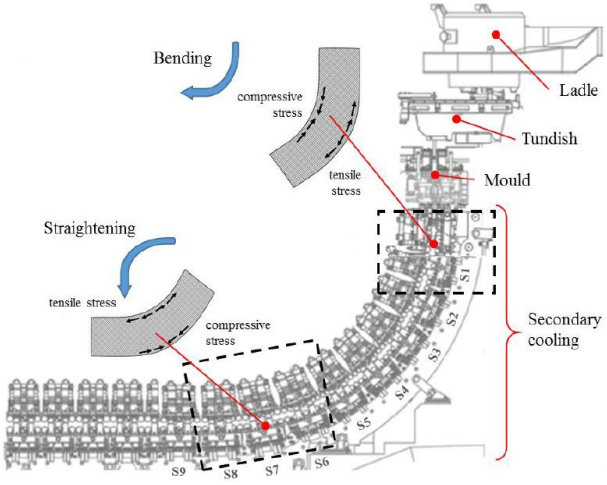

Figure 6: Stresses imposed during straightening and bending [13].

2.2 Physical phenomena: Heat transfer and solidification

During continuous casting the liquid steel melt is solidified into slabs or billets, which are further processed according to the desired shapes. Along the continuous casting process, numerous phenomenon control the overall thermo-mechanical behavior of the steel strand. During this process, every process parameter (e.g., water flow rate, strand geometry, casting speed, etc.), that is directly affecting the casting procedure and final steel quality is necessary to be controlled and monitored. In the next part, some important physical phenomenon such as the heat transfer and solidification that occur during casting process are detailed [14].

2.2.1 Heat transfer

As the heat transport influences the shell strength and thickness, it should be controlled to avoid major crack formation [14]. The narrow gap between the mold walls and the solidifying shell is filled with mold flux. Heat is transferred by radiation and thermal conduction across this interfacial gap. The amount of heat extraction in continuous casting is a dynamic balance between the type of steel, casting speed, mold geometry, coolant type and coolant flow rate [Figure 7] [15].

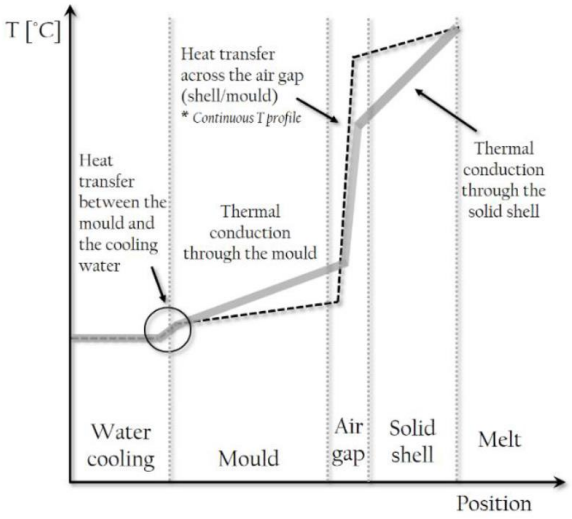

Figure 7: Illustration of temperature distribution the solid metal, mold and melt. [15].

The water-cooling zone is very crucial for the heat transfer, as most of the heat is extracted in this zone. The water cooling zone consists of four different zones: [16]

- Zone 1: Roll contact zone
- Zone 2: dry or low water zone
- Zone 3: Spray zone
- Zone 4: Water pool zone

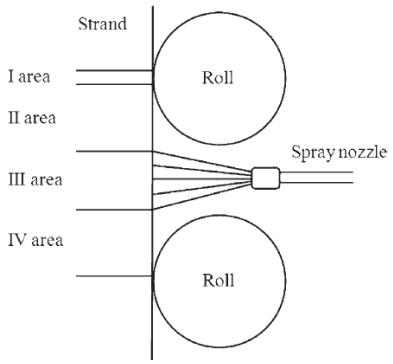

Figure 8: Secondary cooling water zones [16]

In zone 1, the rolls are linked with the strands and extract heat by radiation and conduction. The rollers are continuously cooled by water. Between the roller and the spray, the heat is extracted by conduction and air convection. The spray water zone is the most important zone in term of heat extracted. The heat transfer coefficient *(HTC)* [W.m^{-2}.°C] is empirically determined by [17]:

$$HTC = a * Q^n * c(T) \qquad \textit{(Eq. 1)}$$

Where *a* is an adjustment parameter, *n* is the fitting parameter for the heat flux *Q* and *c(T)* is the term for the Leidenfrost effect. The Leidenfrost effect, which occurs at the endpoint of the nucleate boiling film regime, marks the point where heat transfer is minimized. Below this temperature, the heat transfer increases significantly with decreasing temperature. For this model to effectively describe heat transfer, a thin layer of stream must exist between the solidifying steel and the water sprayed onto the mold surface. This layer ensures a constant heat transfer coefficient over a specific temperature range [18]. However, as the temperature decreases further, the Leidenfrost effect comes into play, significantly altering the heat transfer process. Spray cooling

nozzles employ a high-pressure air and water mixture to achieve uniform cooling. The maximum heat transfer is in the region of stream and water mixture due to which the Leidenfrost temperature value is also increased. *(Eq. 2)* includes other factors, such as velocity and water droplet size [17]:

$$h = 1.90 D_p^{1.1} v_o^{1.1} N^{0.65} \qquad \textit{(Eq. 2)}$$

Where D_p is the diameter of the droplets in the spray, v_o is the impingement velocity and N is the droplet number density.

2.2.2 Solidification and initial growth

The solidification process starts when an atom from the liquid steel occupies a more stable position within a solid alloy lattice. Various methods can be employed to assess the solidification evolution and to determine the solidification lengths as illustrated in Figure 9 [19].

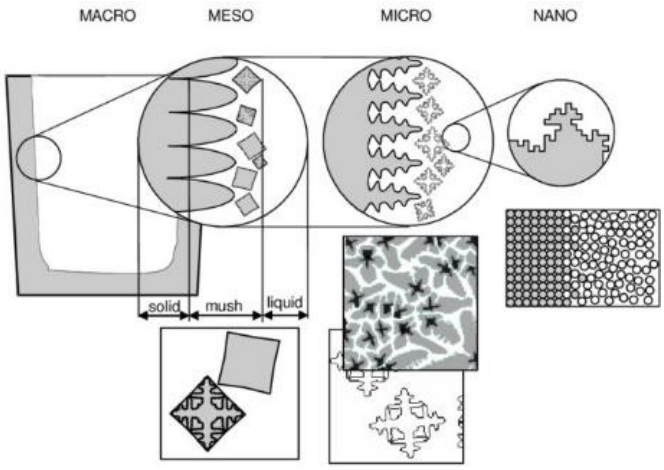

Figure 9: Evolving solidification length: from macro structures to nanoscale [19]

In macroscale (10^{-3} m), the solid and the liquid phases are present and separated by the liquid/solid interface (L/S). In this range, surface roughness, shrinkage, cracks, macro-segregation, casting dimension and cavity can be observed. Mesoscale (10^{-4} m) can just show the solid/liquid interface (S/L) as a line which helps in predicting the grain size in the mesoscale range. The intricate microstructure of grains is revealed at the microscale, ranging from 10^{-6} to 10^{-5} m. The grain size and the solidification structure morphology are very important for the measurement of the mechanical properties and other factors occurring during solidification. Nanoscale (10^{-9} m) shows the atomic level solid/liquid interface (S/L); the nucleation and the growth of the atoms from liquid to solid state can be observed. During nucleation, the stable clusters nucleate in the liquid or at the nearest interface. As a result, these nuclei start to diffuse within the interface and grow atom by atom. Thus, this nucleation and growth of the grains is an important step in determining the morphology and phase transformation of the cast microstructure. The atoms try to

attach themselves in the best available position at the interface and grow. This is based on homogeneous nucleation. If nucleation occurs on the substrate such as mold walls or impurities, that will be heterogeneous nucleation. The atoms try to attach themselves in the best available position at the other interface [19].

The mold wall, a stable surface in continuous casting, facilitates heterogeneous nucleation of crystals. This is the area of primary cooling zone in which the overall shape of strand is defined. The heat is extracted from the strands to facilitate nucleation and undercooling as well as the shell formation. Here liquid is solidified, and microstructure can be controlled. Other factors such as the liquid melt flow, heat flux etc. will interact in the shell formation (Figure 10) [20].

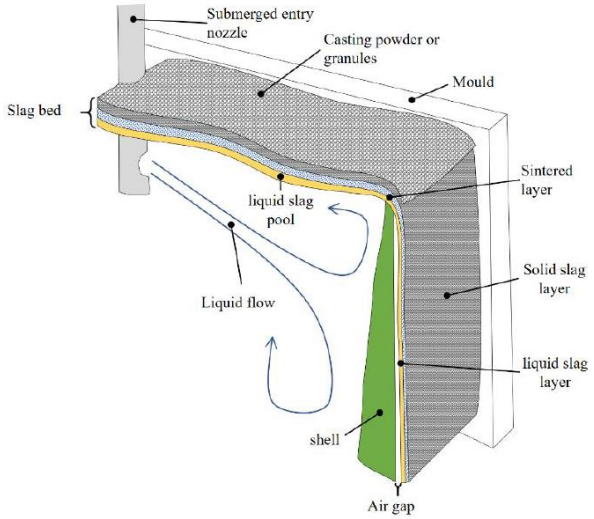

Figure 10: Illustration of the solidification in mold region [20].

Many physical phenomena are present in the solidification at the mold which includes the formation of the surface cracks, micro segregation, phase transformation and microstructure evolution. Solidification initiates at the front interface between the metal which is already solidified and the growing crystal to melt. The solidification front and the undercooling increases with increasing the cooling rate. Undercooling occurs, if the solid is cooled below the equilibrium freezing point, which strongly affects the nucleation and microstructure. The heat extraction rate must be increased to achieve earlier solidification. So, the tree-shaped structure of dendrites can start to grow forward, and secondary arms will grow sideways in opposite direction of the heat flow that is known as dendritic columnar structure. The dendritic arms will grow to form a single crystal lattice [21].

2.3 Steel grade influence on solidification

All the above stated solidification conditions in continuous casting process can influence on the product surface quality and microstructure. It is crucial to comprehend the steel

grade influence to monitor the solidification behavior and the steel specific characteristics of the casting machines under different operating conditions [22].

2.3.1 Solidification mode

The formation of ferrite phase (δ) and the austenite phase (γ) play a crucial role on the solidification behavior and the mechanical properties of steels [Figure 11(a)] [23].

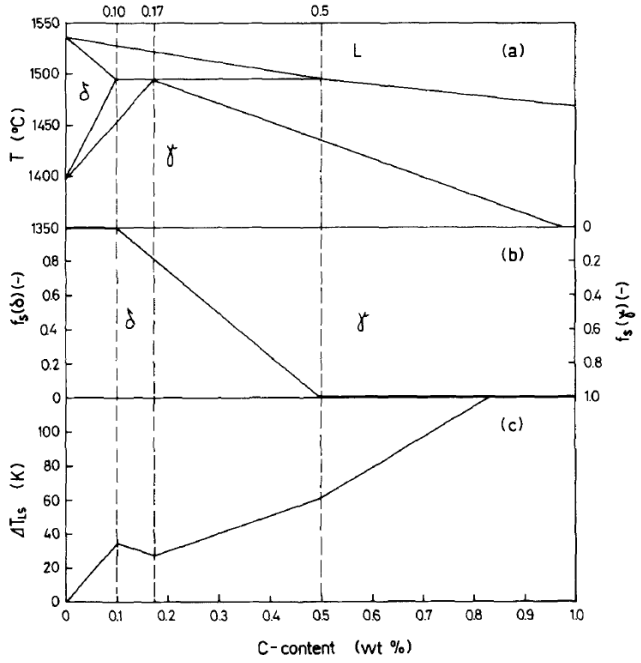

Figure 11: (a) The Fe-C phase diagram at peritectic region. (b) Phase transformation at peritectic temperature: ferrite and austenite coexistence. (c) The temperature interval for solidification: equilibrium solidus and liquidus [23]

As in peritectic range, the amount of liquid, δ and γ phases are shown relative to the temperature and carbon content. Solidification occurs completely in δ phase till 0.10 % carbon. By applying the lever rule for calculating the amount of the ferrite and the austenite in different peritectic ranges along equivalent carbon content, there will be full austenite phase after 0.5 % carbon [Figure 11(b)]. The solidification interval [Figure 11(c)] is a function of local sodification time with respect to the cooling rate. It is possible to calculate the relative proportion of the ferrite and the austenite in the solidified shell by the 'ferrite potential' (FP) term; which is stated as [23];

$$FP = 2.5(0.53 - \%\mathrm{C}) \qquad \textit{(Eq. 3)}$$

In *(Eq. 3)*, if the value of FP is above 1, it refers to the ferritic solidification, while negative values is for autenitic solidification. If the value lies between 0 and 1, it will be a mixture of both the austenite and the ferrite. Many alloying elements are added in the steels depending on the required properties in steel grades. Elements that are austenitic stablizers will move the peritectic point toward the austenite region and stabilize the austenite. While ferritic stabilizers stabilizes the ferritic region by moving the peritectic

point toward the ferrite region. Nickel (Ni) and Chromium (Cr) are the most commonly used alloying element and others are used as equivalent to these two, [23]

$$\mathrm{Cr}_{eq.} = \mathrm{Cr} + 1.37\mathrm{Mo} + 1.5\mathrm{Si} + 2\mathrm{Nb} + 3\mathrm{Ti} \qquad \textit{(Eq. 4)}$$

$$\mathrm{Ni}_{eq.} = \mathrm{Ni} + 0.31\mathrm{Mn} + 22\mathrm{C} + 14.2\mathrm{N} + \mathrm{Cu} \qquad \textit{(Eq. 5)}$$

For the stainless steel grades, $Ni_{eq.}$ to $Cr_{eq.}$ ratio calculates the amount of ferritic potential in solidification The formula for calculating ferritic potential (FP) for stainless steels is; [23]

$$FP = 5.26\left(0.74 - \frac{\mathrm{Ni_{eq.}}}{\mathrm{Cr_{eq.}}}\right) \qquad \textit{(Eq. 6)}$$

Figure 12 illustrates the variations in ferrite and austenite phases proportions among different stainless-steel grades throughout solidification.

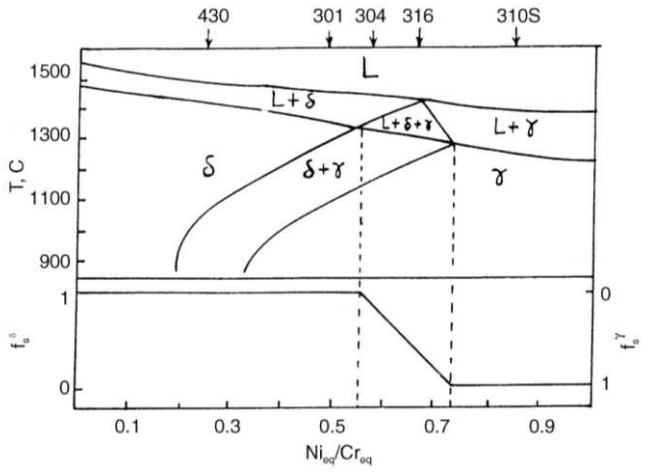

Figure 12: Relative proportion of ferrite and austenite phases among different stainless-steel grades during and after solidification [24].

2.3.2 Classification of steels based on casting parameters

The distinct solidification behaviors of various steel grades highlight the importance of tailoring casting parameters that cater to the specific characteristics of each steel grade. To address this, the common steel grades are categorized into three distinct groups categories based on their solidification behavior and specific quality issues: [24]

Steels with < 0.04 wt. % C and high Si content as well as ferritic or martensitic stainless steels: [24]

- Solidification occurs in the δ region which exists from 100 – 250 °C under the solidification temperature (T_{SA}),
- The overall strand and the solidifying shell show very low creep strength,

- High tendency of bulging of strand and sticking in the mold,
- High chances of inter-columnar cracks in the cast slab which can be clearly seen under rolling operation.

Considering these issues; recommended solution is to employ a glassy slag by maintaining the basicity of the mold powder below 1 to achieve better lubrication and the mold taper should be approx. 0.7 % for accurate casting dimensions.

Steels with 0.08 wt. % - 0.14 wt. % C as well as austenitic stainless steels (specially AISI – 304): [24]

- Solidification occurs in δ region. But at solidification temperature (T_{SA}), δ phase will transform into γ phase.
- The solidifying shell shows high creep strength and is thick.
- Shrinkage can occur and deep cracks can be formed on the surface and subsurface.
- Coarser grains in the cast product can cause embrittlement at 1000-1100 °C. Intergranular cracks can occur on the rolled product.
- Deep oscillation marks can cause surface cracks and lamination in the cast slab.

Considering these issues; recommended solutions are to control the mold heat transfer by using the mold powder (basicity > 1) and the mold taper should be high (0.9 – 1.0 %).

Steels with ≥ 0.25 wt. % C and AISI – 310 SS: [24]

- Solidification occurs through γ mode,
- Higher shrinkage and high chances of micro segregation, which can result in thin shell and formation of deep mushy zone,
- Bulging in strand is high which can result in macro segregation and cracks like center-line cracks and inter-columnar cracks.

Considering these issues; recommended solutions are to keep the large mold taper (0.9 - 1.0%) and decrease the amount of the Sulphur and Phosphorus to achieve a fine-grained microstructure and minimize the likelihood of defects. The ratio of Mn/S should be high to minimize the risk of bulging, and this can be achieved by enhancing the rate of heat removal at the top regions of the strand with smaller diameter rolls. Cracking can be minimized by lowering the casting speed, maintaining low superheat, and keeping the mold taper high.

2.4 Secondary cooling system – Aperam Genk

Aperam's secondary cooling system, developed by the Voelstalpine industries, employ a combination of three different calculation models to dynamically adjust setpoints for the secondary cooling loops every five seconds. These models gather input data specific to the required steel grade and caster configuration to optimize cooling conditions and ensure consistent product quality [25].

2.4.1 DYNASPEED model

The DYNASPEED model is a standard model for the secondary cooling system that actively monitors and updates the strand's actual age (time elapsed since the liquid steel entered in the mold) in real time. This model predicts the optimal water flow rate for each cooling segment, ensuring that the solidifying strand is cooled at the appropriate rate tailored to its current casting speed. The DYNASPEED model's adaptability extends to the selection of cooling strategies, ranging from the average speed strategy, which considers the average casting speed, to the speed strategy, which adopts the cooling procedure based on the current casting speed, and the subject to loop strategy, that accounts the relationship between two loops.

Considering the actual process input data, the DYNASPEED model calculates the cooling loop based on the average casting speed of the strand [Figure 13] [25].

The average casting speed of the strand at the loop '*i*' and time '*t*' is derived by following formula [25]:

$$avCS(i,t) = \frac{\frac{a_i + b_i}{2}}{\frac{1}{b_i - a_i}\int_{a_i}^{b_i} t_{strand}(x,t)dx} \qquad \textit{(Eq. 7)}$$

Where, loop '*i*' refers to a specific section along the length of strand, a_i indicates the distance from the mold level to the starting point of loop '*i*', b_i indicates the distance from the mold level to the end of loop '*i*', *avCS(i,t)* is the average casting speed at loop '*i*' and time *'t', and* t_{strand} shows the time spent by steel in the strand.

Time (t_{strand}) can be measured by cooling model. Strand is divided into small segments (10 cm length) and t_{strand} refers to the center point of each segment. The area segments are shifted according to the casting speed in the model.

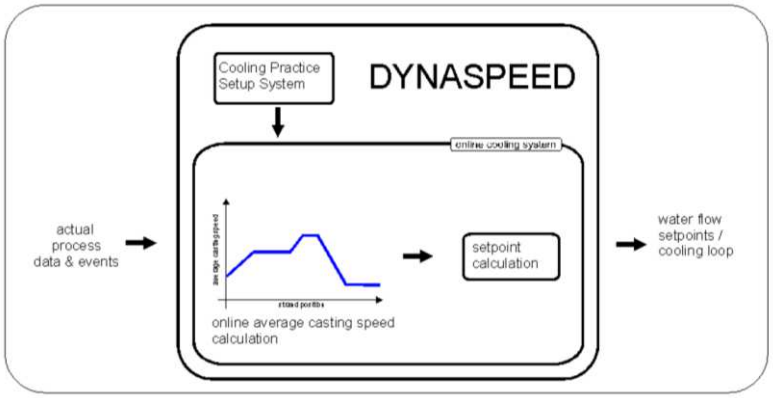

Figure 13: DYNASPEED model – cooling loop calculation based on average casting speed [25]

2.4.2 DYNASHELL model

DYNASHELL model is a standard model for the secondary cooling system that actively assesses and updates the shell thickness profile of the strand in real time, considering

the strand's residence time. This model predicts the optimal water flow rate for each cooling zone, ensuring that the solidifying strand is cooled at an appropriate rate tailored to its instantaneous shell thickness and casting speed. The model's adaptability extends to the selection of cooling strategies, considering the shell thickness strategy, which focuses on the strand's shell thickness, the speed strategy, which considers the current casting speed, and the dependent from loop strategy, which accounts for the relationship between two loops. Furthermore, DYNASHELL possesses information of the position of the point of complete strand solidification, enabling precise control of the cooling process.

Considering the actual process input data, the DYNASHELL model calculates the water flow setpoints depending on the strand shell thickness casting speed [Figure 14]

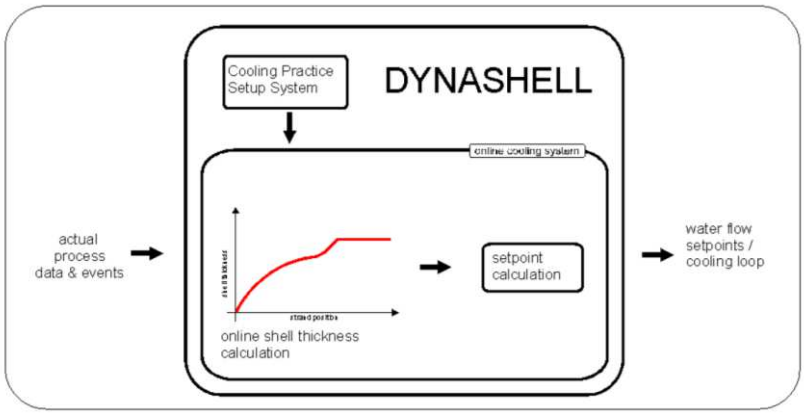

Figure 14: DYNASHELL model – cooling loop calculation based on shell thickness [25]

The shell thickness can be estimated by the following formula:

$$sh(x,t) = \sqrt{k_{mould}(x,t)^2 * t_{mould}(x,t) + k_{strand}(x,t)^2 * t_{strand}(x,t)} \qquad \textit{(Eq. 8)}$$

Where, *sh(x,t)* is the shell thickness at position *x* and time *t*. *K* is the solidification factor for the mold and the secondary cooling region.

2.4.3 DYNACS model

DYNACS model is an advanced model for the secondary cooling system that actively assesses and continuously updates the strand's temperature profile in real time, based on the inputs about the steel grade thermodynamic data, casting speed, and water flowrates. This model calculates the water flow setpoints for each cooling loop, ensuring that the solidifying strand is cooled at an appropriate rate tailored to its dynamic temperature profile and the selected cooling strategy. DYNACS' adaptability extends to a range of cooling strategies, including bulging limiting control, surface temperature control and speed strategy. Bulging limiting control focuses on preventing bulging by factoring the steel shell thickness and ferro-static pressure. Surface temperature control

aims to maintain a specified strand surface temperature in each cooling zone. Speed strategy considers the current casting speed, and is dependent on loop strategy, which accounts for the relationship between two loops. Furthermore, DYNACS possesses information about the strand's thermodynamic state, including the residual internal energy, enabling precise control of the cooling process.

Considering the actual process input data, the DYNACS model calculates the water flow setpoints depending on the temperature profile calculation [Figure 15].

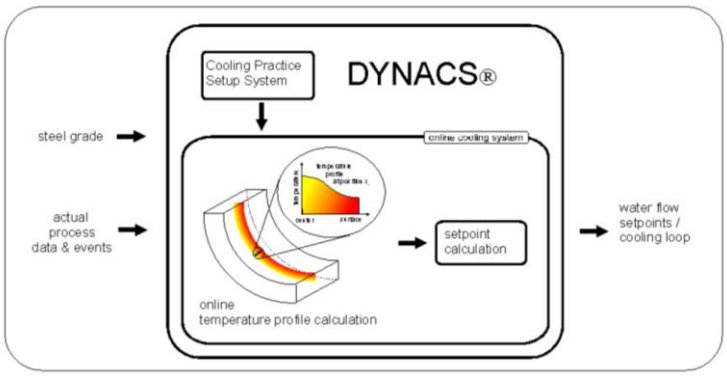

Figure 15: DYNACS model – cooling loop calculation based on temperature profile [25]

The mold heat removal consists of radiation and the theoretical mold heat removal function.

$$radiation(t) + mouldHeatRemoval(t) \quad \textit{(Eq. 9)}$$

For the secondary cooling area:

$$radiation(t) + heatRemovalByWater(t) \quad \textit{(Eq. 10)}$$

It can be calculated by:

$$radiation(t) = \sigma\varepsilon\left(T^4_{surf.}(t) - T^4_{ambientR}\right) \quad \textit{(Eq. 11)}$$

$$MouldHeatRemoval(t) = mhrf\left(T_{surf.}(t)\right) * \left(T_{surf.}(t) - T_{ambientM}\right) \quad \textit{(Eq. 12)}$$

$$heatRemovalByWater(t) = \alpha\left(specFlow(t)\right) * \left(T_{surf.}(t) - T_{ambientW}\right) \quad \textit{(Eq. 13)}$$

Here, *t* is the time, σ and ε are the radiation constants, $T_{surf.}$ is the surface temperature, $T_{ambientM}$ is the ambient temperature for mold, $T_{ambientR}$ is the ambient temperature for the radiation, $T_{ambientW}$ is the ambient temperature for the water flow, mhrf is the function for the heat removal coefficient for the surface temperature and α(specFlow) is a function for heat removal coefficient for the specific water flow.

2.5 CFD modelling

With the advancement in computational modelling, it is convenient to apply complex mathematical equations to simulate and understand the complex phenomenon during continuous casting of stainless steels. The main advantage of using computational models for continuous casting is to simulate and analyze the phenomenon of the material flow, the heat transfer, and the solidification procedure. By using computational modelling, it is easier and reliable to simulate the following phenomenon: [24],[26]

- Heat transfer within the solid and liquid flux layers.
- Superheat transportation by the turbulent steel melt.
- Inclusion transportation in the liquid which includes the inclusions entrapment on walls of the nozzle, the solidifying shell, the gas bubbles, and the top surface, as well as the turbulent interaction and the effect of buoyancy.
- Heat transfer at the meniscus region with the interaction of the solidifying shell, the liquid steel, and the inclusions.
- Overall heat transfers from the tundish to the end of the solidifying steel including different interfaces in the steel solidification.
- Mechanical effect on the water-cooled rollers and the mold walls.
- Detailed analysis of the solidification profile, which also includes the formations of the cracks, dendrites' growth, phase transformation and micro segregation.
- Analysis of the shrinkage of the solidifying steel due to the several reasons related to the steel quality and microstructure.
- The crack formation.

It is difficult to model all the above stated phenomena together. It is more efficient to focus on the essential phenomena and disregard those that are not relevant. Every model is designed to simulate specific phenomena. After choosing the governing equations, they are solved based on the Finite Element Method (FEM) or the Finite Volume Method (FVM) or the Finite Difference Method. After this the model is validated by experimental measurements on the plant or the laboratory scale.

2.5.1 Governing equations: mathematical formulation

For the heat transfer and solidification process, the equation for the conservation of energy according to the First law of thermodynamics is stated as: [27],[28]

$$\rho \frac{\partial H}{\partial t} + \rho \nabla * (\bar{u} H) = \nabla\left(k_{eff.} \nabla \mathrm{T}\right) + Q_L \qquad \textit{(Eq. 14)}$$

Where $\bar{u}$ is the velocity, C_p is the specific heat, $K_{eff.}$ is the effective conductivity and Q_L is a source term. Enthalpy (H) is calculated by the sum of latent heat (ΔH) and sensible heat (h)

$$H = \Delta H + h \qquad \textit{(Eq. 15)}$$

Similar, the sensible enthalpy is defined as:

$$h = h_{ref.} + \int_{T_{ref.}}^{T} C_p dT \qquad \textit{(Eq. 16)}$$

where h_{ref} and T_{ref} are the values for the reference enthalpy and the reference temperature. Similarly, the latent heat content (ΔH) is defined as: [28]

$$\Delta H = L\beta \qquad \textit{(Eq. 17)}$$

Where L is the latent heat of material for liquid fraction (β).

The source term (Q_L) has two term which represents the latent heat term and the convective term, which can be shown as:

$$Q_L = \rho L \frac{\partial f_s}{\partial t} + \rho L \bar{u}_{pull} * \nabla f_s \qquad \textit{(Eq. 18)}$$

During the continuous casting, the strand moves with constant velocity ($\bar{u}_{pull}$). The casting speed is linked with the cooling rate and cooling practice. At that zone, the solid fraction (f_s) will be equal to one. It will change according to the casting speed. Similarly, the sum of the solid fraction and the liquid fraction (β) will be one. The mathematical formula for calculating liquid fraction (β) is given below: [28]

$$\beta = \begin{Bmatrix} 0 & if\ T < T_{solidus} \\ \dfrac{T - T_{solidus}}{T_{liquidus} - T_{solidus}} & if\ T_{solidus} < T < T_{liquidus} \\ 1 & if\ T > T_{liquidus} \end{Bmatrix} \qquad \textit{(Eq. 19)}$$

The equation of continuity is based on the conservation of mass, which is shown as: [29]

$$\frac{\partial}{\partial x_i}(\rho u_i) = 0 \qquad \textit{(Eq. 20)}$$

For the velocity vector (u_i) is shown as:

$$u_i = \frac{\partial u}{\partial x} + \frac{\partial v}{\partial y} + \frac{\partial w}{\partial z} \qquad \textit{(Eq. 21)}$$

Where u, v, and w are the velocity components in 3D coordinates.

Similarly for law of conservation of momentum is expressed by the Navier-Stokes equation: [16]

$$\frac{\partial}{\partial t}(\rho u) + \rho \nabla (uu) = -\nabla P + \nabla\{\mu_{eff.}(\nabla * u)\} + \rho + S \qquad \textit{(Eq. 22)}$$

Where effective viscosity ($\mu_{eff.}$) is the sum of the dynamic viscosity (μ_l) and the turbulent viscosity (μ_t). In the case of enthalpy-porosity technique, the porosity is dependent on the amount of liquid fraction. If there is only solid zone, then porosity will be zero, otherwise the porosity is represented as the amount of liquid fraction. The term 'S'

donates the momentum sink value, that gives the amount of solidified material that flows downward at constant velocity. This *'S'* can be expressed as: [29]

$$S = \frac{(1-\beta)^2}{(\beta^3 - \xi)} A_{mush}\left(\bar{u} - \bar{u}_{pull}\right) \quad \textit{(Eq. 23)}$$

A_{mush} is the constant value for the mushy zone which represents the damping amplitude. If this value is higher, there will be a gradual drop of the velocity value till zero during the solidification of steel. In the momentum sink *'S'* term; the relative velocity of liquid melt and solid is considered instead of the absolute velocity of liquid. The ***k - ε*** turbulence model is more suitable for simulating the turbulence in system; provided by the turbulence velocity term:

$$\mu_t = \rho C_\mu \frac{k^2}{\varepsilon} \quad \textit{(Eq. 24)}$$

Here ***ε*** is the dissipation rate for the turbulent kinetic energy *(k)*. There are two partial differential equations that can be considered: [29]

For the turbulent kinetic energy *(k)*:

$$\rho \frac{\partial k}{\partial t} + \rho(\nabla k u) = \nabla\left(\alpha_k \mu_{eff} \nabla k\right) + G_k + \rho\varepsilon + S_k \quad \textit{(Eq. 25)}$$

For the dissipation rate *(ε)*:

$$\rho \frac{\partial \varepsilon}{\partial t} + \rho(\nabla \varepsilon u) = \nabla\left(\alpha_\varepsilon \mu_{eff} \nabla \varepsilon\right) + C_{1\varepsilon} \frac{\varepsilon}{k} G_k - C_{2\varepsilon}^* \rho \frac{\varepsilon^2}{k} G_k \quad \textit{(Eq. 26)}$$

The sink term '*S'* is added to all the turbulence models. Similarly, the S_k is linked with the momentum sink term (Eq. 23):

$$S = \frac{(1-\beta)^2}{(\beta^3 - \xi)} A_{mush} \varphi \quad \textit{(Eq. 27)}$$

Similarly, ***φ*** represents the turbulence quantity, which is to be solved for the *k*-model or the ε-model.

2.5.2 Boundary conditions: procedure and determination

The result of the computational modelling is strongly influenced by the initial and the boundary condition for the computational domain. A reliable and correct heat transfer model includes correct demonstration of the thermal boundary conditions. If the boundary conditions are accurate for one caster, then it can be used in other related casters, as multiple specifics are relevant for similar casting machines. Steel grades have a high influence on the thermophysical properties thus resulting in changing the boundary conditions. As the behavior of steel grade changes with temperature, it will affect the cooling and the solidification procedure of the steel. Considering the boundary conditions, it covers all the aspects related to in and out flow, the symmetric boundaries, the periodic boundaries, and the solid walls.

In recent years, there is a lot of research performed on the heat transfer modelling for continuous casting. Most of the simulated models are for offline steady state continuous casting, in which strand temperature is dependent on the water spray flow rate, the strand geometry, the casting speed, the mold heat removal, and the steel grade. Figure 16 shows the schematic representation of the temperature field model in the continuous casting strand in the perspective coordinates.

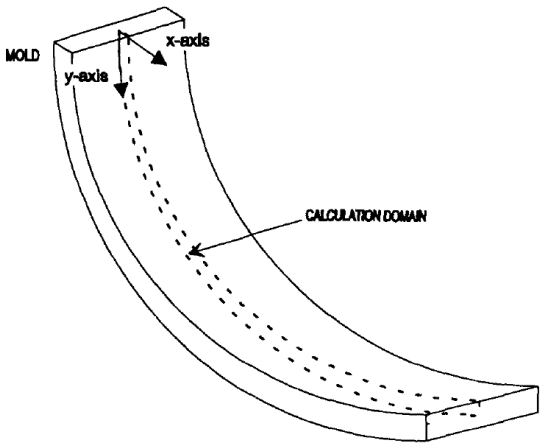

Figure 16: 2-D schematic representation of temperature field model [29]

The inlet conditions is the temperature of steel before entering the mold: [29]

$$T(r,\theta,t)|_{t=0} = T_{cast} \qquad \textit{(Eq. 28)}$$

Heat flux boundary condition is used for the mold region:

$$\vec{q} = \frac{\rho_\omega C_\omega W \Delta T}{S} \qquad \textit{(Eq. 29)}$$

Here, q is the average heat flux. ρ_ω and C_ω are the density value and the specific heat of the water. S is the surface area for the water-cooling spray rate W.

For the calculations of accurate boundary conditions for the secondary cooling zones, there is a lot of work already performed varying from model to model. Various models differ from the water-cooled convective heat transfer and the additional radiative term. For the radiative heat transfer (h_{rad}) term:

$$h_{rad} = \sigma\varepsilon(T_s^2 + T_{ext}^2)(T_s + T_{ext}) \qquad \textit{(Eq. 30)}$$

Emissivity (ε) is a term related to the strand formation and is dependent on the carbon content. T_{ext} is the external temperature and T_s is the surface temperature.

For the convective term in heat transfer model, the water-cooled spray nozzles are the major reason for the solidification and the heat withdrawal from the mold. The heat

removal rate is correlated to the amount of the water sprayed on the surface. Similar to this [30], an experimental setup has been developed by Horsky et al. and Wendelstorf et al. [31] to understand and experiment the heat transfer co-efficient for the water spray nozzles. It is calculated as a function of water flow rate, nozzle geometry and orientation, and surface temperature. It is believed that an optimization of the water spray nozzles is the correct way to obtain a feasible and reliable boundary conditions [31].

The heat transfer coefficient between the solidifying shell and the mold region is related to the thermal resistance and followed by the equation for radiative heat transfer:

$$h = \frac{1}{{}^{1}/_{h_1} + {}^{1}/_{h_2} + {}^{1}/_{h_3} + {}^{1}/_{h_4}} + h_r \qquad \textit{(Eq. 31)}$$

h_1 represents the heat transfer coefficient between the mold and the mold flux. The value is assumed to be approximately 3000 W.m^{-2}.$^{\circ}$C [32]. Similarly, h_2 is the region for the air gap and the thermal conductivity of air, with a value of 0.1 W.m^{-2}.$^{\circ}$C. h_3 is the region for the thermal conductivity and thickness of the mold flux, with value of 1.0 W.m^{-2}.$^{\circ}$C. h_4 will be the value from the solidifying shell to the mold flux and can vary with the mold flux physical state. While h_r represents the radiation heat transfer coefficient through air gap.

The literature data about the boundary conditions for mushy zone at different regions is calculated as: [33]

At the inlet of Submerged Entry Nozzle (SEN):

$$v_x = 0, \quad v_y = 0, \quad v_z = v_{inlet}, \quad T_{inlet} = T_L + \Delta T,$$

$$k_{inlet} = 0.03 v_{inlet}^2, \quad \varepsilon_{inlet} = k_{inlet}^2/(0.005d)$$

Here v is the velocity at different point coordinates at SEN. T_L is the liquidus temperature and ΔT donates the superheat temperature, while d is the inner diameter of SEN.

On the strand:

$$V * n = 0, \quad (n * \nabla)|V| = 0, \quad n * \nabla \emptyset = 0$$

Here, n is the normal vector to the scalar quantity $(\emptyset)$ which can be either T, ε or k.

At outlet of the strand: *[34]*

For velocity component (u): $n * \nabla \emptyset = 0, \ (n * \nabla)|V| = 0,$

For velocity component (w): $|\sum(\rho V * A)|_{outlet} = |\sum(\rho V * A)|_{inlet}$

u, v, and w are the velocity components taken in the Cartesian coordinate system.

For strand surface below the exit of mold: *[34],[35]*

$$V * n = 0, \quad t * V = V_{cast}, \quad h = \frac{700W}{m^2}\ ^{o}C, \quad T_{\infty} = 30\ ^{o}\text{C}$$

Here *t* is considered as a tangent vector to the surface of the strand.

Mold surface: *[34],[35]*

For *the top and bottom of the mold part:* $h = \frac{1.1\,W}{m^2}\ ^oC, \quad T_\infty = 30\ ^oC$

Above meniscus region in hot area*:* $h = \frac{11\,W}{m^2}\ ^oC, \quad T_\infty = 1500\ ^oC$

In area between cooling region and the mold: [35]

$$\frac{hD_H}{k_w} = 0.23\ Re_w^{0.8}\ Pr_w^{0.4} \qquad \textit{(Eq. 32)}$$

Here, k_w shows the thermal conductivity for the cooling water, Re_w is the Reynold number for cooling water and Pr_w is the Prandtl number for the cooling water and D_H is the hydraulic diameter.

Boundary conditions: material properties

After defining the boundary conditions, it is suggested to define the assumptions to eliminate the unnecessary demands of the model. The main aim of the model is considered, and all other unnecessary areas are neglected. After this, the relevant material data is collected as shown in Table 1 [36]

Table 1: Material Properties based on boundary conditions [36].

Material property	Unit	Value
Density of Steel	$kg.m^{-3}$	7200
Thermal conductivity	$W.m^{-1}.K^{-1}$	41
Viscosity of Liquid Steel	$kg.m^{-1}.s^{-1}$	0.0067
Specific heat	$J.kg^{-1}.K^{-1}$	750
Solidus Temperature	K	1770
Liquidus Temperature	K	1800
Latent heat	$J.kg^{-1}$	272000
Casting speed	ms^{-1}	1.0 - 1.4
Mushy zone	-	100000
Liquid steel superheat	K	15 - 25

2.5.3 Validation and monitoring

Related to the validation of the computational model, the model can either be validated by the experimental techniques or by the plant measurements in the plant or laboratory depending on the model conditions. After validation, it can be used for the optimization of the heat transfer and solidification in the continuous casting process. Regarding the validation of the heat transfer model, there is a lot of research performed on different computational models for the validation at different point of casting stands, which are stated as:

- If the heat withdrawal from the mold is considered, one point is to do inverse modelling and measure the change in temperature in the mold which can be compared from the integral heat flux data from the measurement in a plant. Plant measurement can be done by measuring the change in temperature of the cooling water which can be used in the casting process. This step will provide the data about the initial part of the solidification model. [37]
- Breakout shells can be used for measuring the thickness of the shell, depending on the availability. The measurement can be taken at different positions and different regions of the caster. The breakout issue during casting can occur due to the unsteady casting conditions, so this type of validation model can be used with caution and is very limited.
- Temperature can be measured by the pyrometer installed in the continuous casting plant setup. Which can detail about the temperature at different regions and at different lengths of the strand. However, it is necessary to install pyrometer correctly to get the correct measurement and avoid any related error. In the case of dragged thermocouples, it is necessary to have a well-defined contact between the strand and the reference thermocouple.

2.5.4 Previous research on continuous casting modelling

Much research work has been performed on the performance and calibration of the various casting parameters for continuous casting process. Many thermal stress computational models are investigated for the slab casting, billet casting, thin slab casting and beam blanks[27],[38]–[40]. The first computational thermal stress model was investigated by Brimacombe, and Grill [38],[39] in a two-dimensional billet section under plane stress, which is later used in a continuous casting plant. Initially these kinds of models analyze the crack formation behavior to identify the crack initiation in billet sections. Those models have been proven to be very useful in determining the material fracture at high temperature, but to use a high mesh was a big issue at that time due to the limitations of the computational power. Rammerstorfer et al. [26] designed a thermo-viscoelastic-plastic stress model for slab caster by adding a separate creep function in a transient one-dimensional plane. [26] Kristiansson et al. further used Rammerstorfer et al. model with combination of thermal and stress computation in two-dimension (2-D) billet section considering the interfacial gap between the solidifying shell and the mold and modeled the temperature dependent properties of the austenitic and the ferritic steels by featuring different creep constants [26]. Kelly et al. [41] developed an axisymmetric model and performed elastic-stress analysis on the mold region and elastic-plastic stress analysis on the billet to model the thermal stresses to investigate the influence of carbon content on the formation of different longitudinal cracks.

Many researchers have designed different models, from 1D to 3D, to simulate the process parameters and optimize the heat transfer and solidification process. In 2006, Alizadeh et al. [42] designed a two-dimensional finite volume numerical model (FVM)for slab caster and validated that model by measuring the slab temperature in real conditions. This model simulated the heat transfer and solidification profile by adopting the enthalpy-porosity technique, in which the liquid fraction (f_L) is a major modification of the enthalpy formulation. The two-dimensional finite volume model can simulate the shell

thickness profile, temperature profile at different regions of the strand and the mold on basis of the energy and mass balance equations. B. Abd El-Bary and Y.A. Rihan, [43] performed a FVM technique to study the heat transfer and temperature profile in the continuous casting mold. The model used *k-ε* turbulence for determining the temperature profiles. [Figure 17]

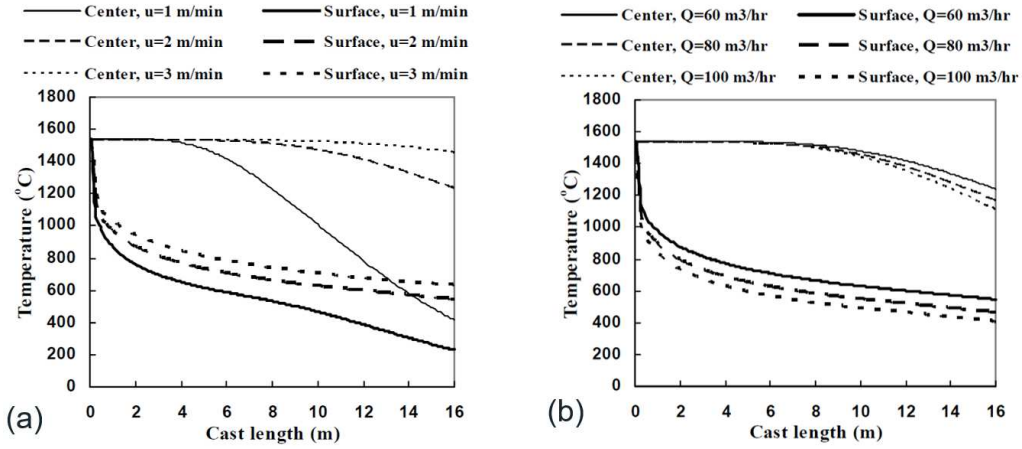

Figure 17: (a) Temperature distribution along different cast length at the center and the surface with different casting speed and same cooling rate (Q=60 $m^3.hr^{-1}$). (b) Temperature distribution along different cast length at the center and the surface with different cooling rate and same casting speed (u_c=2 $m.min^{-1}$) [43]

Louhenkilpi et al. [44] used a finite difference dynamic three-dimensional (DYN3D) model to simulate the temperature field in the caster. This model used the heat transfer coefficient to simulate the change in temperature between the solidifying shell and the mold walls. Zhao [45]modified the Louhenkilpi model to predict the heat transfer in the secondary cooling region by using the conservation of energy equation and Navier stokes equation in the inverse heat transfer problem (IHTP) model by using nonlinear estimate method. Later in 2011, Botoka and Sowa et al. [35] used the Fourier Kirchhoff system to simulate the heat flows during the solidification in the mold region. The velocity fields at different regions during solidification is measured by this model. Considering the requirement for thermophysical parameters, Botoka and Sowa et al. modified the model by adding the temperature dependent effective superheat term ($C_{eff.}$) in Fourier Kirchhoff system: [44]

$$\nabla.(\lambda\Delta T) - C_{eff.}\frac{\vartheta T}{\vartheta t} - C_{eff.}\nabla T.V = 0 \qquad \textit{(Eq. 33)}$$

$$C_{eff.}(T) = \rho_{LS}c_{LS} + {}^{\rho_S L}/_{(T_L - T_s)} \qquad \textit{(Eq. 34)}$$

Zhao and Chen [45] used the finite element model to simulate the heat transfer in the continuous cast beam billets, and validated the results with the infrared sensors installed in the plant. This model was used to optimize the secondary cooling zone for the beam blank caster. The surface quality of the final products was improved by considering the validated results of this model [Figure 18].

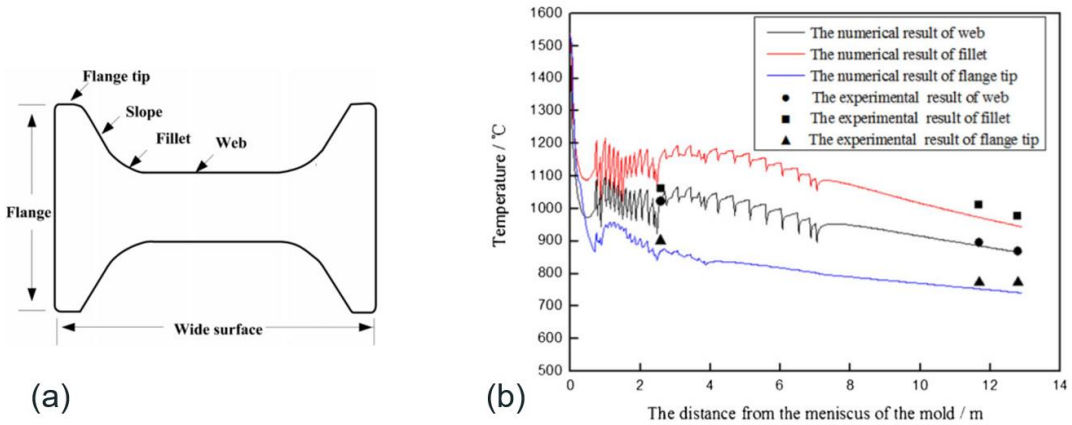

Figure 18: (a) Beam Blank cross-section. (b) Comparison of the simulated results at the different areas of the beam blank with the actual measurements data from the continuous casting plant. [45]

There is a lot of improvement in the computational models for determining the heat transfer and solidification behavior in the continuous casting process. Boehmer et al. [35] used a combined model of the inhouse heat transfer model in a three dimension (3-D) heat flow model and the ADINA thermal stress model (2-D) to simulate the performance in the continuous caster in plane stress. The elastoplastic constitutive modelling approach was used combining the stress-rate-dependent strength and plasticity. AMEC2D model, [32] is a transverse slice model that was designed by Lee et al. to simulate the superheat phenomena in the liquid steel from the tundish for the beam blank casting which is a result of a simple fluid-flow model and an elastic-viscoplastic behavior. Park et al. used this transverse slice model for billets and assumed plane stress and overlooked the influence of superheat to simulate the effect of mold corner radius on shell growth and the formation of cracks in billets [32].

Table 2: Overview of previous research and insights gained

Contribution	Modelling techniques	Phenomenon	Insight
Brimacombe and Grill [38],[39]	Two-dimensional billet sections under plane stress	Thermal stress modelling	Mechanism of crack formation and avoid reheating
Rammerstorfer et al. [26]	One-dimensional transient modelling for slab section	Thermo-viscoelastic-plastic stress model with creep function	Addition of creep function
Kristiansson et al. [26]	Two-dimensional (2-D) travelling slice model for billet section	Stepwise coupling of thermal and stress computations	Temperature dependent properties of austenitic and ferritic steels
Kelly et al. [41]	Axisymmetric model for round billets	Elastic stress analysis, elastic-plastic stress analysis	Effect of carbon content on the propensity of longitudinal cracks

Alizadeh et al. [42]	Two-dimensional finite volume numerical model (FVM) for slab	Enthalpy-porosity technique	Heat transfer and solidification profile
B. Abd El-Bary and Y.A. Rihan, [43]	FVM technique	*K-ε* turbulence model	Temperature profile and industrial data validation
Louhenkilpi et al. [44]	Finite difference dynamic three-dimensional (DYN3D) model	Heat transfer coefficient	Temperature distribution in the strand and the mold walls
Zhao [45]	Inverse heat transfer problem model	Conservation of energy equation and Navier stokes equation	Calculation of secondary cooling heat transfer by nonlinear estimate method
Zhao and Chen [45]	2-D transient finite element model	Accurate boundary conditions	Optimize the secondary cooling scheme for beam billets
Boehmer et al. [35]	3-D heat flow model and the ADINA thermal stress model (2-D)	Elastoplastic constitutive model, stress-rate-dependent strength, and plasticity	Performance in the continuous caster in plane stress
Lee et al. [32]	AMEC2D model - transverse slice model for beam blank casting	Fluid-flow model and an elastic-viscoplastic behavior	Superheat phenomena in the liquid steel
Park et al. [32]	AMEC2D model - transverse slice model for billets	Plane stress and neglected the effect of superheat	influence of mold corner radius on the shell growth and the formation of cracks in the billets

Researchers have used different modelling techniques aiming to address issues such as crack formation, strand distortion or bending, finer microstructure, and efficient heat transfer and solidification. Computational modelling has emerged as an effective approach to optimize the casting process by developing a realistic model that bypasses the need for costly and time-consuming practical casting trials. Numerous models have been developed to simulate the continuous casting process, there remains a need for more advanced models that can effectively optimize casting parameters and minimize the casting defects, ultimately increasing the production efficiency.

Chapter 3: Methodology

In this chapter, we outline the methodology employed to calculate different thermophysical parameters for Aperam's standardized steel grades and implement them in the DYNACS model and the CFD model. This primary focus is to evaluate how input parameters affect the results that these computational models produce. Additionally, a thorough review is conducted to assess the effects of changing the steel grade composition, more specifically transitioning from steel grade 304L to 316L, on the outcomes of the cooling model.

This research contributes to a better understanding of the dynamic interaction between steel composition and cooling processes, providing key insights for the field of metallurgical engineering. The following sections will delve into the methodology's complexities, covering data collection, modeling techniques, and statistical analyses - all of which are essential for the thorough explanation of the research objectives.

3.1 Calculation of thermophysical parameters

Steel grades 304L and 316L are selected as the primary materials for this study. The heat transfer and solidification profile in continuous casting is directly influenced by the thermophysical properties such as solidus and liquidus temperature, density, thermal conductivity, specific heat, and latent heat of the material. The values of a thermophysical parameter over a range of temperatures and steel compositions can be calculated by a regression relation or by experimental laboratory measurements. Regression relations give us only an approximate estimate of the thermophysical parameters. Instead of relying on regression relations or experimental laboratory measurements, the calculations of thermophysical properties for the given chemical compositions were conducted utilizing two software tools: Thermo-Calc and IDS (Inter-Dendritic Solidification).

Thermo-Calc (thermodynamic calculation) is a computational software tool used for precise thermodynamic and phase equilibrium calculations. Thermo-Calc is used to predict and study different material properties, including but not limited to phase diagrams for multicomponent systems, thermodynamic properties, precipitation, and solidification. Since it allows for precise predictions and insights into the thermodynamic behaviour of materials, Thermo-Calc has become an essential tool for researchers and engineers in the fields of materials science, metallurgy, and related ones [46]. In this research Thermo-Calc 2022a version is used to calculate different thermodynamic properties. The chosen database for this study is TCS Steel and Fe – alloys (TCFE-12).

Similarly, IDS (Inter-Dendritic Solidification) was created as early as 1984 in the Finnish Metallurgy Laboratory of the Technical University in Helsinki. IDS is based on a combination of empirical approach and physical models. The model calculates thermophysical properties such as density, thermal conductivity, specific heat capacity,

viscosity, enthalpy, liquidus and solidus temperature, etc. The results were experimentally validated on many steel grades with different chemical compositions. The first version of this program was commercially available in 1997 for the DOS operating system. Later, other versions were created. More about the IDS program is available in [46]. In this research, IDS version 2.0 is used to calculate different thermophysical properties.

The chemical compositions of steel grades 304L and 316L provided by Aperam are shown in Table 3:

Table 3: Aperam Steel grade for study

wt. %	C	Mn	Si	Cr	Ni	Mo	Cu	N
304L	0.025	1.45	0.4	18	8	0.3	0.3	0.075
316L	0.025	1.25	0.5	16.5	10	2.05	0.3	0.04

Solidus and liquidus temperature:

Solidus and liquidus temperature are important thermophysical parameters that define the temperature range within which a material transitions between solid and liquid phases. These values are calculated by modelling the phase equilibrium calculations within the alloy based on its chemical composition. The software uses the CALPHAD (Calculation of Phase Diagrams) method to accurately predict phase boundaries.

Density:

The density (ρ) of homogeneous materials can be determined by the ratio of mass (m) to volume (v); ρ=m/v. The density of the solid and liquid phases is calculated by using the phase compositions obtained by Thermo-Calc calculations. The relationship of phase compositions and densities is available in the TCFE database. The density of the mushy zone (semi-solid) was estimated by interpolation method, accounting the phase fraction variation within the zone.

Thermal conductivity:

Thermal conductivity (λ) characterizes the ability of a substance to conduct heat, whether it is in a solid, liquid, or mushy state. In liquids, we consider conduction only if the medium is at absolute rest. Like density, the thermal conductivity values for different phases are calculated by phase compositions obtained by Thermo-Calc.

The main heat transfer in the continuous casting process is heat transfer by conduction. However, the convection of the liquid core manifests itself by a change in conductivity, therefore the so-called effective thermal conductivity $\lambda_{eff.}$ Includes the movement of particles within the liquid phase and mushy zone. The effective thermal conductivity is then calculated using linear relation, accounting for the changing phase distribution during phase transitions [47]:

$$\lambda_{eff.}(T) = \lambda_s(T) f_s + A\lambda_l(T)(1 - f_s) \quad \textit{(Eq. 35)}$$

where λ_s (T) and λ_L (T) are the conductivity of respectively the solid and liquid phase. F_s is the proportion of the solid phase in the mushy zone. *A* is a constant that varies between 1 – 8. However, it is difficult to determine this value precisely because it depends on the type of caster, and it is different in the mushy region and in the secondary zone depending on the movement and turbulence of the melt.

Specific heat capacity:

The specific heat capacity *(c)* expresses the amount of heat needed to heat 1 kilogram substance by one kelvin. It can be expressed using the relation c = Q/mΔT, where Q is the heat energy (joules), m is the mass of material (kg), and ΔT is the change in temperature (kelvin). Specific heat values are calculated using the thermodynamic database available in the TCFE database, accounting the phase fractions within the alloy.

Latent heat:

Latent heat is a critical parameter in thermal analysis. It is a measure of heat absorbed or released during the phase transition. The values are calculated from the phase fraction data derived from the established thermodynamic database.

The calculated thermophysical parameters from Thermo-Calc and IDS serve as important inputs for DYNACS and CFD models. These parameters will help in predicting the heat transfer and solidification behavior of steel grade 304L and 316L during cooling process.

3.2 Aperam model simulations

The thermophysical parameter's values calculated by Thermo-Calc and IDS 2.0 are used as input values in DYNACS model of Aperam cooling model to calculate the temperature and the solidification process of the steel grades. The available input parameters in the steel grade section of the DYNACS model are the chemical composition (minimum, aim, and maximum ranges), the cooling caster description related to the strand type (slab, bloom, billet), the strand mode (single, twin, triple), the casting sizes of strand (width and thickness), the spray nozzle size (width of the cooling spray), the solidus and liquidus temperature, the densities for the solid, mushy and liquid state, the latent heat, and the solidification factor. The DYNACS model uses the steel grade properties to calculate the heat removals and temperature of the strand. The aim surface temperature is adjusted in the model as an input and based on that temperature, the cooling model predicts the water flow rate for every segment. So cooling practice consists of controlling the casting speed and the desired surface temperature. The Aperam model uses the same set of thermophysical parameters (density, thermal conductivity, specific heat, and latent heat) for 304L and 316L steel grade, and the profile for these two steel grades already exist in

Aperam cooling model. Based on the calculated thermophysical parameters from Thermo-Calc and IDS, the DYNACS model uses special integral method, as indicated in the model description to simulate accurate and reliable temperature and solidification results.

The strand and caster information must be defined and selected before starting the simulation. In this case, there is just one strand, so 'strand 1' is selected for all simulations, and 'DEMO – DYNACS' is selected as caster. Further in the dynamic simulation window, the cooling practice is based on the steel grade. The width of the slab for this simulation varies in the range of 1.04 m to 1.59 m, and a thickness of 200 mm. The casting speed for the simulation is adjusted in the range of 1.2 $m.min^{-1}$ to 1.4 $m.min^{-1}$ and the superheat is kept between 15 °C to 40 °C.

The next step is to initialize the setup and select the option 'Start cast' to start the casting process. A window showing the secondary cooling relevant information will appear, where we can see the graphical representation of calculated shell thickness along the strand, calculated liquidus isotherm, the strand age, the average surface temperature in different segments of the casting. The simulated results of the average surface temperature at zone 7 is compared with the pyrometer data, that is positioned in the start of zone 7 in Aperam continuous casting plant [Figure 19], and the calculated overall shell thickness are taken for solidification profiling to compare the influence of thermophysical parameters in different process conditions.

3.3 CFD modelling study on heat transfer and solidification

This section describes the modelling of the mold and secondary cooling region for the continuous caster in Aperam. The CFD solver process solves the calculations based on the specific boundary conditions by considering the provided material properties. In this section, the development of the CFD model is given, including the methods applied to improve the convergence and their effect on the model.

3.3.1 Geometrical model of the continuous caster

In the field of metallurgical simulations, the modelling of continuous caster poses a unique set of challenges. Ansys modules offer the flexibility to model in one-, two- or three-dimensional domains. A two-dimensional model is considered most appropriate for this research based on several factors. The two-dimensional modelling approach in terms of heat transfer and solidification captures all the complex aspects of heat transfer and solidification process. The accurate boundary conditions are calculated for the mold and the secondary cooling region, this will result in accurate temperature and solidification predictions in a two-dimensional plane. Besides the metallurgical reasons, the two-dimensional modelling approach is simpler than the three-dimensional modelling approach, saving computational resources, and leading to faster calculations with good accuracy.

A two-dimensional heat transfer and solidification model is designed to analyze the cooling strategy happening in the mold and the secondary cooling region of the continuous caster. The model is developed by considering the actual dimensions of the continuous caster in Aperam with the overall length of ~ 23 m, the detailed dimensions are shown in [Table 4]. The geometry for the mold and the secondary cooling part is created using the "Ansys – Design Modeler" – geometry drawing software coupled with Ansys Fluent in Ansys Workbench. The caster consists of the mold and the secondary cooling region, and the overall caster is divided into eight different segments to apply separate boundary conditions for each segment. There is an additional section highlighted in between zone 6 and 7 named as 'zone – pyrometer' to compare the temperature values with the pyrometer; that is positioned in the start of zone 7 in Aperam – plant. The start of the mold region is defined as inlet and end of the secondary cooling region is defined as outlet. The 'Design Modeler' geometry drawn in x-y plane is shown in [Figure 19].

Table 4: Dimensions of the mold and secondary cooling region

	Mold	**Secondary cooling region**							
Segments	**Zone 1**	**Zone 2**	**Zone 3**	**Zone 4**	**Zone 5**	**Zone 6**	**Zone – pyrometer**	**Zone 7**	**Zone 8**
Zone length (m)	0.370	0.743	1.741	1.919	3.838	3.841	0.2	3.543	7.056

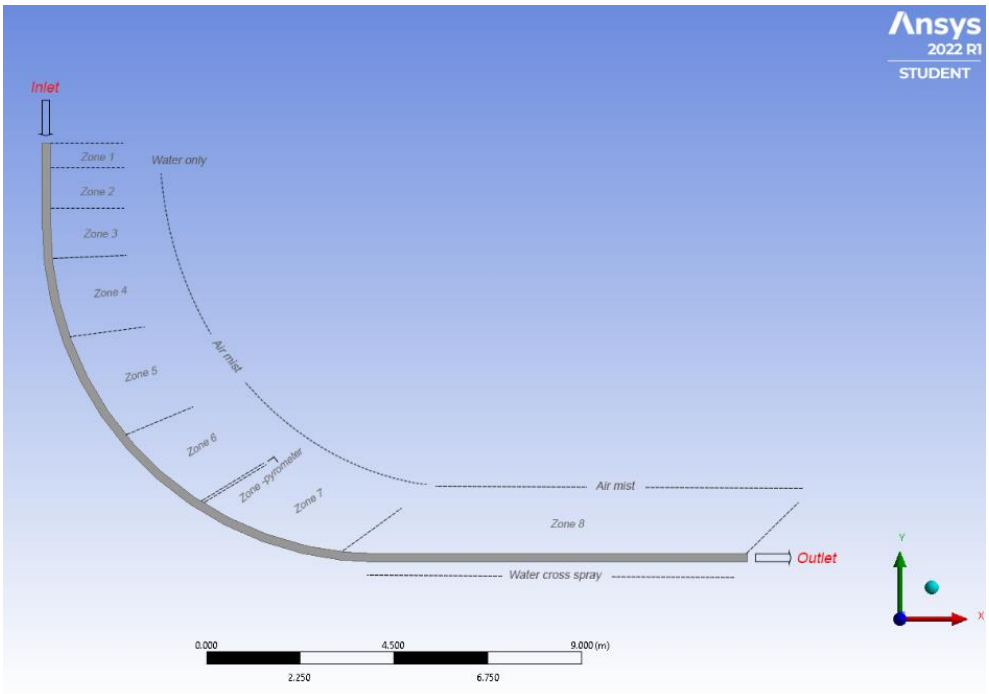

Figure 19: Geometry of continuous casting mold and secondary cooling region

3.3.2 Meshing

The physical space of the imported geometry from 'Design Modeler' (Ansys – Fluent) is divided into many geometric elements, called geometric cells. The 2-D geometric cell consists of rectangular, triangular, and quadrilateral elements. All the defined parts of the geometry such as the inlet, outlet, mold, secondary cooling region, and zone 7 are selected as the surfaces for generating a finer mesh. There are two types of geometric grids in meshing, structured and unstructured. Structured mesh is a simple and efficient way of connecting the grid points and expressing in a 2-D or 3-D array. It is also efficient in solving computational algorithms and decreases computational time. In the case of complex geometry, creating a structured mesh can take longer time but it will result in high accuracy. The unstructured mesh consists of hybrid or mixed grids and can include random elements such as triangular, quadrilateral, hexagonal, tetrahedron, hexahedron and prismatic elements. Most commonly, it includes triangular elements in 2-D and tetrahedron in 3-D. This kind of mesh is used in commercial simulation solvers. Due to the complexity of the grid, the unstructured mesh takes more storage space than the structured mesh [Figure 20] [48].

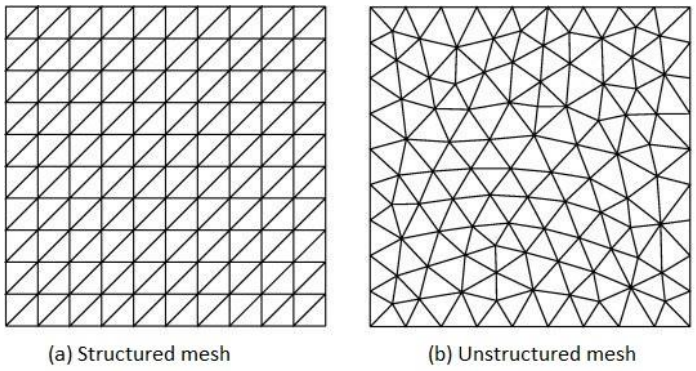

Figure 20: Representation of structured and unstructured mesh [48]

There are a few requirements for a mesh that must be considered for generating a better quality mesh. The numerical stability of the selected model and accuracy of the model is highly dependent on the mesh quality. It is preferred to keep the resolution as high as possible if the grid element number is not limited. But using a higher grid element can result in higher computational costs and causing slower turnaround times. For Ansys student version, the grid elements are limited to 500,000. The grid element should be linked with the next grid element and there should be no overlapping of the elements. The element size is preferably kept low to have an efficient mesh. Different grid refinement techniques can be used to change the grid elements based on the requirement of modelling process. Furthermore, for a better-quality mesh, the grid elements are increased in the areas of interest such as boundary layer, sharp points or edges, and areas of pressure gradient.

In this continuous caster mesh, a structured mesh is generated by using higher grid elements in the areas of interest such as boundary layer, sharp points or edges, and areas of pressure gradient. There is a smooth transition of smaller elements (near the boundary layer) to the larger elements (in the center of the slab) for effective heat transfer results. [Figure 21] shows the mesh distribution in the strand.

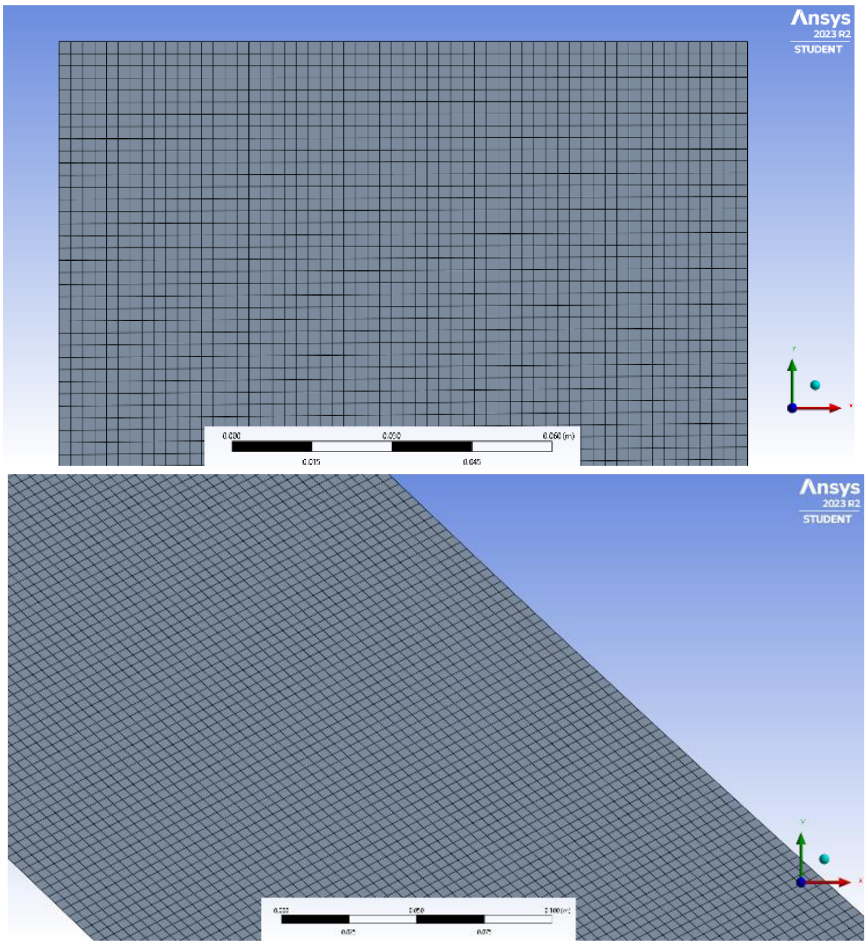

Figure 21: Mesh distribution in the continuous casting strand

Considering the geometry of the continuous caster, the applied methods for refining the mesh are the face meshing and edge meshing. The number of divisions for the edge meshing is 120 divisions. For face meshing, a mapped mesh approach is applied using quadrilaterals. Applying these two methods, the mesh forms a structured grid. The mesh element size is 0.005 m. This will divide the complete geometry into small elements and a structured mesh is properly distributed on the face. The specific details of the mesh quality are provided in [Table 5].

Table 5: Mesh properties and qualities

Mesh properties and qualities	
Number of nodes	394120
Number of elements	387383
Average element quality	0.8661
Average aspect ratio	1.0922
Average skewness	0.15509
Inflation	Smooth transition
Growth rate	1.2

After refining the mesh, the file is converted into a compatible format for the Ansys fluent solver process.

3.3.3 Governing Equations

The fundamentals of computational fluid dynamics (CFD) are based on transport equations. These equations provide a foundational structure that allows researchers to effectively communicate their ideas, implement algorithms in CFD software, and recognize and fix any issues that may come up during simulations. They also give users a common framework for describing and understanding the behavior of fluids. The transport equation explains the movement of a scalar quantity within a fluid. This equation is used in many different fields, including fluid dynamics, heat transfer, and mass transfer. Understanding the transport equation is critical for modelling and predicting the behavior of scalars such as temperature, momentum, or solidification front position – in fluid systems.

Here is the general form of the Navier-Stokes equation:

$$\frac{\partial \rho}{\partial t} = \nabla * (\rho v) - \nabla * \Gamma \nabla v + S \qquad \textit{(Eq. 36)}$$

Where: ρ can be a scalar quantity linking with temperature or concentration, $\partial\rho/\partial t$ is the change of scalar quantity with respect to time, v is the velocity vector, ∇ is the nabla operator representing the divergence of the scalar. Γ is the diffusion coefficient, S is the source or sink term.

To understand the components of the transport equation, it is divided into three individual components:

Convective term ($\nabla*(\rho v)$): The convective term indicates the transport caused by the movement of fluid directly.

Diffusion term ($\nabla*\Gamma\nabla v$): The second term represents the scalar spreading or mixing caused by concentration gradients.

Source term (S): The third term refers to the influence of some external factors such as chemical reactions, mass, or heat transfer from external sources.

For the simulations, ANSYS – Fluent is used; an efficient and reliable platform for solving Multiphysics problems. The software can discretize the Navier-Stokes equations to predict the heat transfer and solidification process of the CFD model by following the law of conservation of mass, law of conservation of energy and law of conservation of momentum in the defined fluid and solid domains. The simulation setup uses the following equations:

Law of conservation of mass (Continuity equation):

Considering the Navier-Stokes equation (Eq. 36), the continuity equation follows the conservation of mass in the computational domain, which ensures that no mass is created or destroyed during the simulation.

$$\frac{\partial \rho}{\partial t} + \nabla * (\rho v) = 0 \qquad \textit{(Eq. 37)}$$

Where ρ is the density of fluid, and v is the velocity of fluid.

Law of conservation of energy:

Considering the Navier-Stokes equation (Eq. 36), the energy equation is linked with the heat transfer processes involving the molten metal, the solidified part within the mold and the secondary cooling zones that includes both the fluid and the solid domain. Energy equation considers all the linked heat transfer mechanisms such as conduction, convection, and radiation.

$$\rho C_{p.eff} \left(\frac{\partial T}{\partial t} + v * \nabla T\right) = \nabla * (k \nabla T) + S \qquad \textit{(Eq. 38)}$$

Where $C_{p.eff}$ is effective specific heat capacity, k is the thermal conductivity and S is the source term.

Law of conservation of momentum:

Considering the Navier-Stokes equation (Eq. 36), the law of conservation of momentum considers all the accounting forces acting on the domain such as pressure, gravitational forces, and viscous forces.

$$\rho \left(\frac{\partial v}{\partial t} + v * \nabla v\right) = -\nabla \mathrm{p} + \mu_{eff.} \nabla^2 v + \rho g \qquad \textit{(Eq. 39)}$$

Where p is the pressure, and $\mu_{eff.}$ is the effective viscosity.

Turbulence modelling:

Turbulence in continuous casting is a crucial aspect to be considered during modelling heat transfer and solidification in the mold and secondary cooling region. Turbulent flow enhances the heat transfer within the molten steel which helps in homogenizing the steel composition and is crucial for achieving the desired solidification profile and preventing defects. Using an accurate turbulence model is necessary to predict the accuracy of result and validate the casting conditions. Standard k-ε turbulence model is widely used in the heat transfer and solidification CFD modelling of continuous casting due to its minimal complexity and high precision. Considering the Navier-Stokes equation (Eq. 36), the standard k-ε model consists of two-equations linked in the eddy-viscosity turbulence model that implements these two transport equations for turbulent kinetic energy (k) and the turbulent dissipation rate (ε), are given as follows [49]:

$$\frac{\partial}{\partial t}(\rho k) + \nabla * (\rho U k) = \nabla * \left[\left(\mu_l + \frac{\mu_t}{\sigma_k}\right) \nabla k\right] + G_k + G_b - \rho \varepsilon + S_k \qquad \textit{(Eq. 40)}$$

$$\frac{\partial}{\partial t}(\rho\varepsilon) + \nabla * (\rho U\varepsilon) = \nabla * \left[\left(\mu_l + \frac{\mu_t}{\sigma_\varepsilon}\right)\nabla\varepsilon\right] + C_{1\varepsilon}\frac{\varepsilon}{k}(G_k + C_{3\varepsilon}G_b) - C_{2\varepsilon}\rho\frac{\varepsilon^2}{k} + S_\varepsilon \quad \textit{(Eq. 41)}$$

$$\mu_t = \frac{\rho C_\mu k^2}{\varepsilon} \quad \textit{(Eq. 42)}$$

$$S_k = \frac{(1-f_L)^2}{\left({f_L}^3 - \xi\right)} A_{mush}\varphi \quad \textit{(Eq. 43)}$$

Where G_k and G_b show the turbulence kinetic energy generated due to velocity gradients, and buoyancy. M_t is the turbulent viscosity. $C_{1\varepsilon}$, $C_{2\varepsilon}$, and $C_{3\varepsilon}$ are constants, and the recommended values are 1.44, 1.92 and 0.09. σ_k and σ_ε are turbulent Prandtl numbers for turbulent kinetic energy (k) and the turbulent dissipation rate (ε) and the recommended values are 1.0 and 1.3 [49].

For standard k – ε turbulence model in the ANSYS – Fluent model interface, the necessary model constants linking with the initial and boundary conditions such as the turbulent kinetic energy (k) and the turbulent dissipation rate (ε) are calculated based on above equation (Eq. 42). The solver then solves the turbulence behavior with the other governing equations to calculate the temperature distribution and solidification behavior. The standard k – ε model has proven to be efficient in modelling a wide range of Multiphysics problems including continuous casting [50]. This model is an effective option among researchers and engineers due to its optimal accuracy. The k – ε model has some limitations such as its sensitivity to initial boundary conditions and unable to predict the flow features accurately such as recirculation and separation. Despite these limitations, the standard k - epsilon model is still a useful tool for investigating turbulence in continuous casting.

Solidification modelling:

Modelling the solidification process is a major step in the continuous casting process. Solidification modelling helps in predicting the solidification front, the formation of the mushy zone or growth of solidified crust. The enthalpy porosity technique is used in simulating the solidification process as it provides the actual representation of the phase changing from liquid to solid and help in tracking the solid-liquid interface. One additional parameter "liquid fraction (f_L)" is added in the energy and momentum conservation equation to include liquid and solid phase fraction in the domain.

The momentum equation (Eq. 39) is modified by adding the porosity term ($1\text{-}f_L$) to estimate the liquid-solid phase change in the solidification process:

$$\rho\left(\frac{\partial v}{\partial t} + v * \nabla v\right) = -\nabla \mathrm{p} + \mu\nabla^2 v + \rho g + (1-f_L)f_m \quad \textit{(Eq. 44)}$$

Where f_m represents the momentum sink in the source term.

The energy equation (Eq. 38) is modified by adding the latent heat term, to calculate the thermal energy transfer during the liquid-solid phase change. For this specific heat capacity term is replaced by effective superheat capacity ($C_{p\ eff.}$)

$$\rho C_{p\,eff.}\left(\frac{\partial T}{\partial t} + v * \nabla T\right) = \nabla * (k\nabla T) + S \qquad \textit{(Eq. 45)}$$

$$\rho C_{p\,eff.} = C_p + L\frac{\partial f_L}{\partial T} \qquad \textit{(Eq. 46)}$$

Where L is the latent heat of fusion.

The liquid fraction (f_L) is the ratio of the liquid phase present in the total volume of the calculated domain. The value of the liquid fraction ranges from 0 (completely solid) to 1 (completely liquid). The liquid fraction can be calculated by the lever rule and given as follows:

$$f_L = 1 - f_S = \begin{Bmatrix} 0 & if\ T < T_S \\ \dfrac{T - T_S}{T_L - T_S} & if\ T_S < T < T_L \\ 1 & if\ T > T_L \end{Bmatrix} \qquad \textit{(Eq. 47)}$$

Where f_S is the solid fraction. T_L and T_S are the liquidus and solidus temperature.

In the computational modelling of the solidification process, the mushy zone parameter in the momentum sink equation (Eq. 43) is an important parameter to be calculated. A_{mush} represents a mushy zone constant, which is dependent on several parameters such as temperature gradient across the mushy zone, solidification kinetics, and dendritic arm spacing (λ_2) [49].

$$A_{mush} = \mu_l + K_o \qquad \textit{(Eq. 48)}$$

$$K_o = \frac{180}{\lambda_2^2} \qquad \textit{(Eq. 49)}$$

Where μ_l is the laminar viscosity and λ_2 is the dendritic arm spacing.

The enthalpy porosity technique is implemented by enabling the solidification model in the ANSYS – Fluent interface. All the material properties are specified such as melting temperature, latent heat, specific heat capacity, solidus, and liquid temperature. The solver automatically calculates the liquid fraction based on the provided material properties, energy, and momentum equations accordingly. The enthalpy – porosity technique is very efficient in calculating the solidification profile and keeping the track of solid – liquid interface, however, this technique has some limitations such as, it considers the uniform temperature gradient in the overall computational domain, inability to calculate the dendritic growth. Despite these limitations, the enthalpy-porosity technique is still an efficient technique in determining the solidification profile of continuous casting process.

3.3.4 Boundary conditions

The boundary conditions define the behavior of the liquid and solid domains at the boundaries of the computational domain. It is necessary to accurately define the boundary conditions to get an effective and converged simulation result. For simulating the continuous casting process in the two-dimensional domain, the selection of boundary conditions for the inlet, mold, secondary cooling region, and outlet are discussed in this section. The secondary cooling region is segmented into different segments for implementing different boundary conditions in every segment.

Inlet boundary condition:

The molten steel enters the computational domain from the inlet, so the inlet boundary condition describes the flow behavior as the steel enters the mold region. The following parameters are important to define here:

Velocity: The velocity of the steel refers to the casting speed and the cross section of the computational domain. The velocity can be specified as a constant velocity or as a function of time. For all the simulations, the velocity is set to be a constant velocity.

$$velocity = 1.2\frac{m}{min}, 1.3\frac{m}{min}, 1.4\frac{m}{min}$$

Temperature: The temperature at the inlet boundary condition refers to the temperature of the steel while entering the mold region. The temperature values should be defined from the experimental data or the literature values. The transmission of superheat in the molten steel should be considered for the temperature value.

$$T = T_{casting} + T_{superheat} \qquad \textit{(Eq. 50)}$$

Where superheat values range from 15 °C to 40 °C.

Turbulence: The turbulence parameters such as turbulent kinetic energy (k) and the turbulent dissipation rate (ε) are calculated based on the empirical correlation (Eq. 42) for standard k-ε turbulence model.

Mold boundary condition:

The mold boundary condition is defined according to the interaction of steel melt with the solidifying shell and mold walls. The boundary condition is linked with the heat transfer and friction between the solidifying shell and mold walls. The simplified heat flux boundary condition is implemented for the mold region [29], which is stated as [51]:

$$q_m = \left(268 - \beta\sqrt{\frac{l}{V_{cast}}}\right) * 10^4 \qquad \textit{(Eq. 51)}$$

$$\beta = \frac{1.5 * (2{,}680{,}000 - \overline{q})}{\sqrt{\frac{L_m}{V_{cast}}}} \quad \textit{(Eq. 52)}$$

$$\overline{q} = \frac{\rho_w C_w W_L \Delta T}{S_c} \quad \textit{(Eq. 53)}$$

Where q_m is the heat flux (Wm^{-2}), β is the empirical coefficient, l is the distance of the steel melt from meniscus (m), V_{cast} is the casting speed ($mmin^{-1}$), L_m is the mold length (m), $\overline{q}$ is the mean heat flux, ρ_w is water density (kgm^{-3}), C_w is the specific heat of water ($Jkg^{-1}K^{-1}$), W_L is the water flow rate (Ls^{-1}), ΔT is the change in temperature of water while flowing through the mold (K), and S_c is the contact area between the mold walls and liquid steel (m^2).

Secondary cooling region (SCR) boundary condition:

The secondary cooling region is divided into different segments to implement different boundary conditions which highly depends on the heat removal by cooling nozzles. The HTC_{SCR} is defined as a convective heat transfer coefficient based on the correlation of water spray, radiation and rolling and is defined as:

$$\boldsymbol{HTC_{SCR}} = HTC_{spray} + HTC_{radiation} + HTC_{rolling} \quad \textit{(Eq. 54)}$$

For calculating the heat transfer coefficient for water spray, the correlation from the literature study is used [52]:

$$HTC_{spray\,.\,top\,face} = \frac{1570\omega^{0.55}(1 - 0.0075(T_{spray} + 273.15))}{\alpha} \quad \textit{(Eq. 55)}$$

Where $HTC_{spray\,.\,top\,face}$ is the water spray heat transfer coefficient for the top face of strand ($Wm^{-2}K^{-1}$), ω is the spray cooling flux ($Lm^{-2}s^{-1}$), T_{spray} is the temperature of the cooling water spray (K) and α is the machine dependent calibration factor.

The heat transfer coefficient for the bottom face is modified by the correlation [52]:

$$HTC_{spray\,.\,bottom\,face} = (1 - 0.15\,cos\theta)HTC_{spray\,.\,top\,face} \quad \textit{(Eq. 56)}$$

The radiative heat transfer coefficient can be calculated as:

$$HTC_{radiation} = \varepsilon\sigma(T_{surface}^2 + T_{ambient}^2)(T_{surface} + T_{ambient}) \quad \textit{(Eq. 57)}$$

$$\varepsilon = \frac{0.85}{[\,1 + \exp\,(42.6 - 0.02682T_{surface})^2} \quad \textit{(Eq. 58)}$$

Where $HTC_{radiation}$ is the radiant heat transfer ($Wm^{-2}K^{-1}$), ε is the emissivity of steel, σ is the Stefan – Boltzmann constant [$5.67x10^{-8}$ $Wm^{-2}K^{-4}$], and $T_{surface}$ and $T_{ambient}$ are temperature of surface and ambient temperature in Kelvin.

The heat transfer coefficient for the roll contact can be calculated by this correlation:

$$HTC_{rolling} = \frac{K * V_{cast} * sin\alpha}{\omega * \sqrt{A_{roller}}} \quad \textit{(Eq. 59)}$$

Where: K is the thermal conductivity of the roll material ($Wm^{-2}K^{-1}$), α is the arc of roll contact (radians), V_{cast} is the casting speed (ms^{-1}), ω is the spray cooling flux ($Lm^{-2}s^{-1}$), A_{roller} is the contact surface area of rollers (m).

This formula assumes that the heat transfer is constant between the slab and contact rollers.

Outlet boundary condition:

The outlet boundary condition is defined by specifying the flow behavior at the outlet of computational domain. For these simulations, the pressure outlet is used with the turbulence parameters derived for the empirical correlation such as turbulent kinetic energy and turbulent dissipation rate.

Table 6 provides an overview of the boundary conditions for the CFD model that are used in different region that have been discussed in detail in this section.

Table 6: Boundary conditions for the CFD model

Region	Boundary condition	Details
Inlet	Velocity inlet	$T = T_{casting} + T_{superheat}$ Turbulence parameters: k and ε
Mold	Heat flux	$q_m = \left(268 - \beta\sqrt{\frac{l}{V_{cast}}}\right) * 10^4$
Secondary cooling region	Heat transfer coefficient (HTC_{SCR})	$HTC_{SCR} = HTC_{spray} + HTC_{radiation} + HTC_{rolling}$
Outlet	Pressure outlet	Turbulence parameters: k and ε

3.3.5 Solution procedure and convergence:

The solution procedure of CFD model is based on the combined framework of Navier-Stokes equations and the turbulent k-ε model to simulate the heat transfer and solidification results. The choice of solution procedure depends on the complexity of the problem, the required accuracy, and the available computational resources. Typical

solution procedures involve the discretization of the governing equations, the linearization of the resulting discrete equations, and the use of iterative solvers to obtain the approximate solutions. In ANSYS-Fluent, various solution procedures are available, such as pressure-based or density-based solvers, coupled or segregated solvers, and implicit or explicit time integration methods. The choice of the solution procedure should be guided by the specific requirements and challenges of the continuous casting process.

The chosen modelling approach considers the energy, viscosity, and solidification modules to perform heat transfer and solidification simulations. The energy module is activated to control the transfer phenomena in the casting process, considering conduction and convection. This is necessary to precisely predict the temperature distribution in the mold and secondary cooling region. The viscous (standard k-ε) model is used to accurately predict the robustness in the flow conditions. To correctly solve the near-wall region, the scalable wall function feature was used, which will ensure the accurate prediction of heat transfer and solidification behavior to the mold walls. Similarly, to control the solidification process, the solidification and melting model is activated to control the phase transition from liquid to solid. Mushy zone constant is defined (A_{mush}) to control the formation of mushy zone based on the above-mentioned equations. It is necessary to include and calculate the pull velocities for continuous casting process. The pull velocity is calculated for just one iteration in the solution and then deactivated, which will automatically calculate the pull velocity based on first iteration [53].

All the simulations are started in the steady state using the default pressure-based solver. This solver is due to its reliability and effectiveness in solving flow regimes. The simulations are run for 1500 iterations, making sure the steady state solution is achieved. This step acts as an initialization step for running the simulation in the transient state analysis. This is effective to get the time dependent behavior of the system. This transient simulation setup gives more realistic estimation of heat transfer and solidification process over time happening in the continuous casting process. The transient setup is effective in predicting the behavioral changes in the system by using different casting speeds and superheat. The time step size is kept low to 0.1 second to get converged results.

Following the same solution procedure by changing the desired material properties, inlet conditions (velocity and superheat), and other affecting conditions, all the simulations are performed, and results are saved for the interpretation.

Chapter 4: Results and discussion

4.1 Thermophysical parameters of steel grades 304L and 316L

Different thermophysical parameters are calculated by Thermo-Calc and IDS 2.0 for the provided steel compositions of the steel grades 304L and 316L and are compared with the Aperam parameters (Table 7 and Table 8). The comparative analysis highlights the observed variations in the material properties, such as the solidus and liquidus temperatures, the density, the thermal conductivity, the specific heat, and the latent heat, by using different calculation tools and with the default used values.

Table 7: Comparison of the thermophysical parameters for steel grade 304L between the values used by Aperam and as calculated by Thermo-Calc and IDS 2.0

Parameter	Unit	Aperam	Thermo-Calc	IDS 2.0
Solidus temperature	°C	1385	1428	1398
Liquidus temperature	°C	1456	1460	1456
Density (solid)	$Kg.m^{-3}$	7200	7246	7312
Density (mushy)	$Kg.m^{-3}$	7200	7080	7239
Density (liquid)	$Kg.m^{-3}$	7200	6892	6983
Conductivity (solid)	$W.m^{-1}.K^{-1}$	33.5	31.2	32.8
Conductivity (mushy)	$W.m^{-1}.K^{-1}$	37.8	29.5	31.8
Conductivity (liquid)	$W.m^{-1}.K^{-1}$	60.5	17	28
Specific heat (solid)	$J.kg^{-1}.K^{-1}$	692	968	732
Specific heat (mushy)	$J.kg^{-1}.K^{-1}$	710	1032	757
Specific heat (liquid)	$J.kg^{-1}.K^{-1}$	729	1096	793
Latent heat	$KJ.kg^{-1}$	270	265	201.2

Table 8: Comparison of the thermophysical parameters for steel grade 316L between the values used by Aperam and as calculated by Thermo-Calc and IDS 2.0

Parameter	Unit	Aperam	Thermo-Calc	IDS 2.0
Solidus temperature	°C	1365	1424	1372
Liquidus temperature	°C	1441	1453	1445
Density (solid)	$Kg.m^{-3}$	7200	7312	7349
Density (mushy)	$Kg.m^{-3}$	7200	7096	7261
Density (liquid)	$Kg.m^{-3}$	7200	6951	6997
Conductivity (solid)	$W.m^{-1}.K^{-1}$	33.5	31.6	33
Conductivity (mushy)	$W.m^{-1}.K^{-1}$	37.8	29.8	32

Conductivity (liquid)	$W.m^{-1}.K^{-1}$	60.5	17.2	27.9
Specific heat (solid)	$J.kg^{-1}.K^{-1}$	692	909	710
Specific heat (mushy)	$J.kg^{-1}.K^{-1}$	710	1121	737
Specific heat (liquid)	$J.kg^{-1}.K^{-1}$	729	1133	779
Latent heat	$KJ.kg^{-1}$	270	268	215.1

The results obtained from Thermo-Calc and IDS 2.0 show significant variations in the values as well as when compared with the Aperam values. Notably for both steel grades, Thermo-Calc calculations give higher values for the solidus and liquidus temperatures, as well as specific heat values when compared with the Aperam values and the IDS 2.0 values. In contrast, IDS 2.0 data situated itself in the medium range, bridging the difference between the Aperam parameters and the Thermo-Calc parameters. Also, there is a considerable difference of conductivity values of the IDS 2.0 and the Thermo-Calc from the Aperam values with a particular focus on liquid conductivity values, which showed the most pronounced differences. Several factors play a role in these variations. Thermo-Calc and IDS 2.0 use different thermodynamic databases, mathematical models, and phase diagrams to calculate the phase changes and other properties of the steel grade. As a result, different models can result in different values.

4.2 Study of DYNACS model

In this section, the effect of the variation of the thermophysical parameters on the steel temperature and the solidification profiles as predicted by the DYNACS model is discussed. The temperature distribution and the solidification behavior helps in understanding the heat transfer mechanism, allowing us to predict and control the casting process accordingly.

4.2.1 Temperature profile

The correct estimation of the temperature distribution is crucial in the continuous casting process because it directly impacts the process efficiency. Therefore, the temperature profiles of steel grades 304L and 316L in zone 7 as obtained by the DYNACS model for the three different sets of thermophysical parameters in Table 7 and Table 8 are shown in *Figure* 22 and *Figure 23*. These temperature values are compared with the real plant data obtained from the pyrometer which is placed in the start of zone 7.

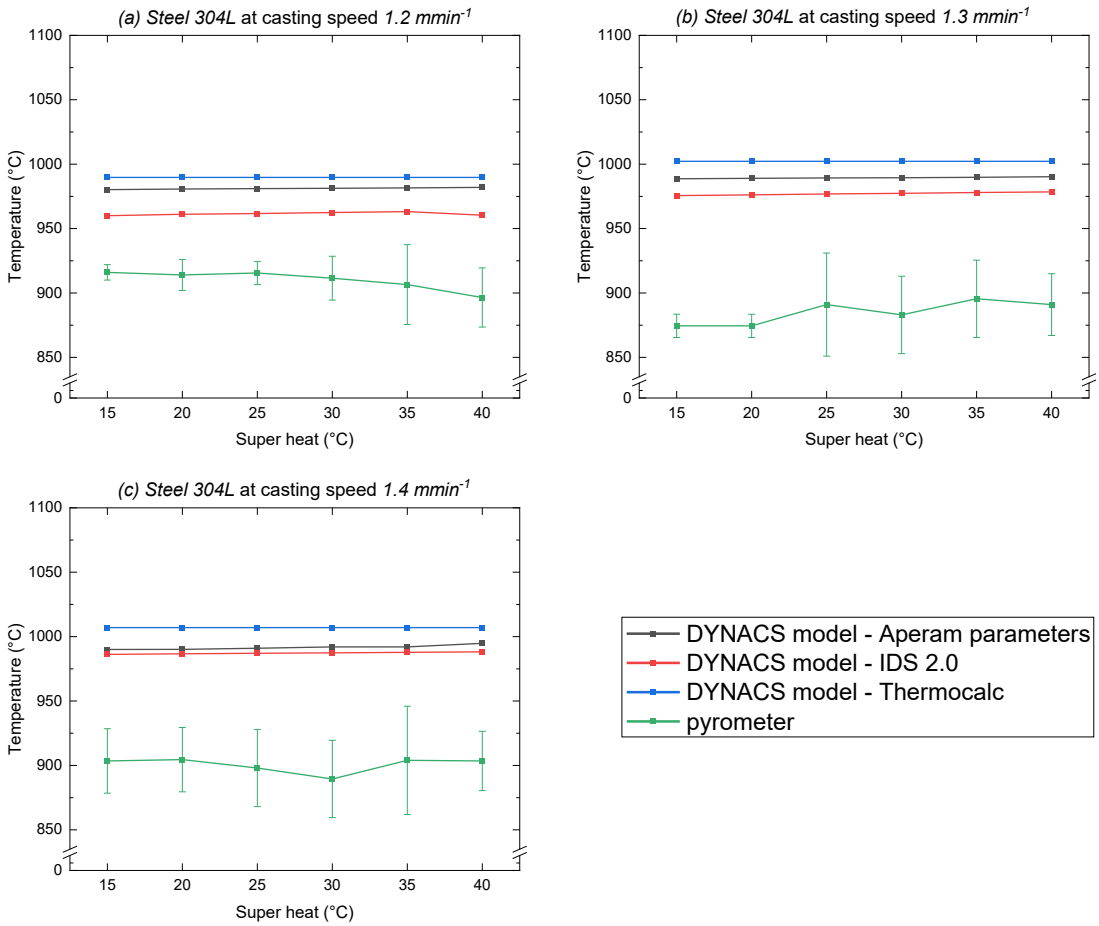

Figure 22: Temperature distribution at zone 7 obtained from the DYNACS model for the steel grade 304L; (a) 1.2 mmin^{-1}, (b) 1.3 mmin^{-1} (c) 1.4 mmin^{-1}

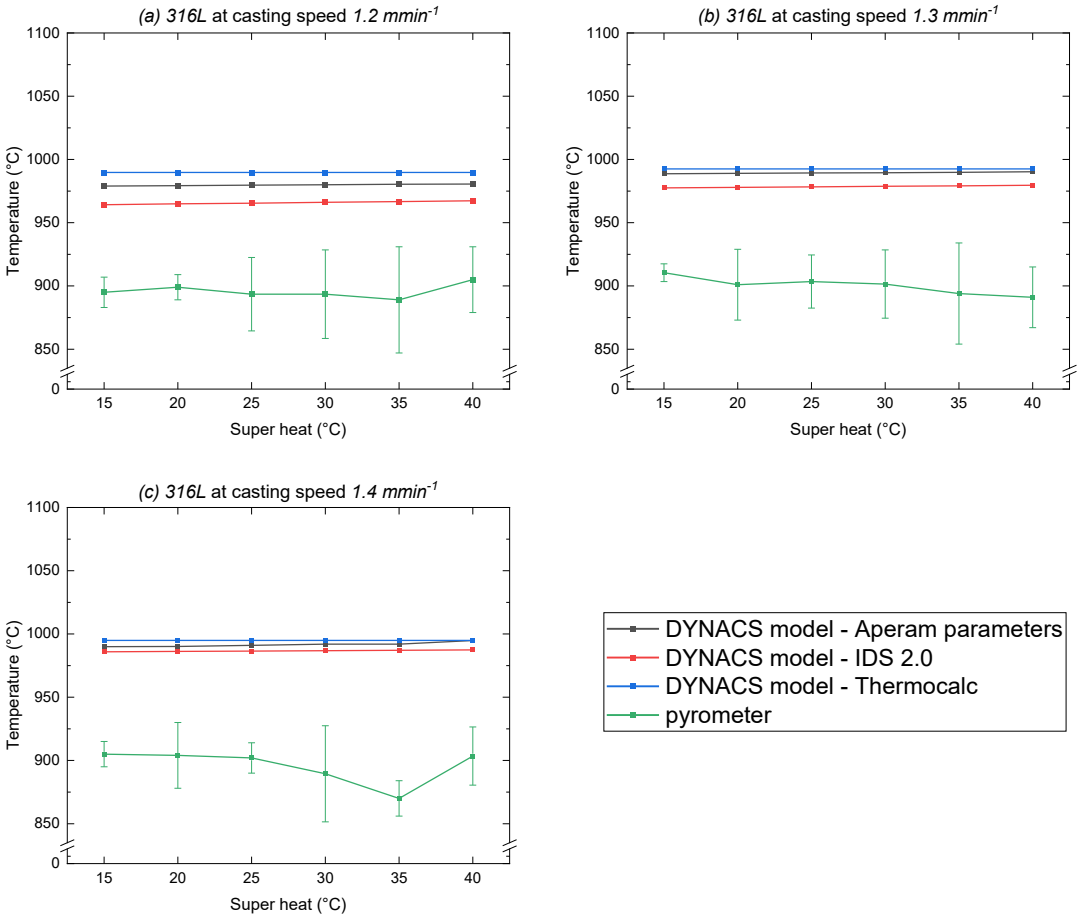

Figure 23: Temperature distribution at zone 7 obtained from the DYNACS model for the steel grade 316L; (a) 1.2 mmin^{-1}, (b) 1.3 mmin^{-1} (c) 1.4 mmin^{-1}

The parameter sets (Aperam, Thermo-Calc, and IDS 2.0) give different temperature values at zone 7 for steel grades 304L and 316L. The predicted temperatures with the DYNACS model for all sets are closely aligned, highlighting the model's sensitivity to minor parameter variations. The IDS 2.0 parameters give the lowest temperature values in the predictions. In contrast, Thermo-Calc parameters give the highest temperature values, whereas Aperam parameters lie intermediate between the two. Notably, the absolute difference across the parameters is minimal but is very high as compared to pyrometer data.

A comparison of steel grades 304L and 316L indicates that the grade 304L has higher temperature values for all three parameter sets. This behavior could be explained by the difference in alloy composition between the two steel grades, especially the higher molybdenum content in steel 316L. The higher molybdenum content in steel grade 316L can affect the kinetics of phase transformations in steel in several ways; increasing the diffusion of carbon or other interstitial elements, formation of complex carbides and increasing the stability of austenite [54]. These factors collectively accelerate the transformation of austenite to ferrite or bainite in steel grade 316L, resulting in faster heat

dissipation and higher overall temperature results in the DYNACS model. These small deviations highlight the robustness of the DYNACS model and suggest that, despite their differences, the three parameter sets produce comparable temperature predictions.

4.2.2 Solidification profile

This section focuses on studying the effect of different sets of thermophysical parameters on the solidification behavior of steel. The goal is to figure out how change in different thermophysical parameters impact the solidification process, ultimately altering the solidification point. *Figure* 24 and *Figure* 25 show the different solidification points along the caster length that are calculated by DYNACS model by using different set of thermophysical parameters and keeping the same cooling rate for same steel grades. The difference in the results highlights the significant impact of the critical parameters on the solidification process. The thermophysical parameters such as the thermal conductivity, the specific heat and the latent heat have a direct impact on the heat transfer, energy requirement, and heat absorption, during the solidification process.

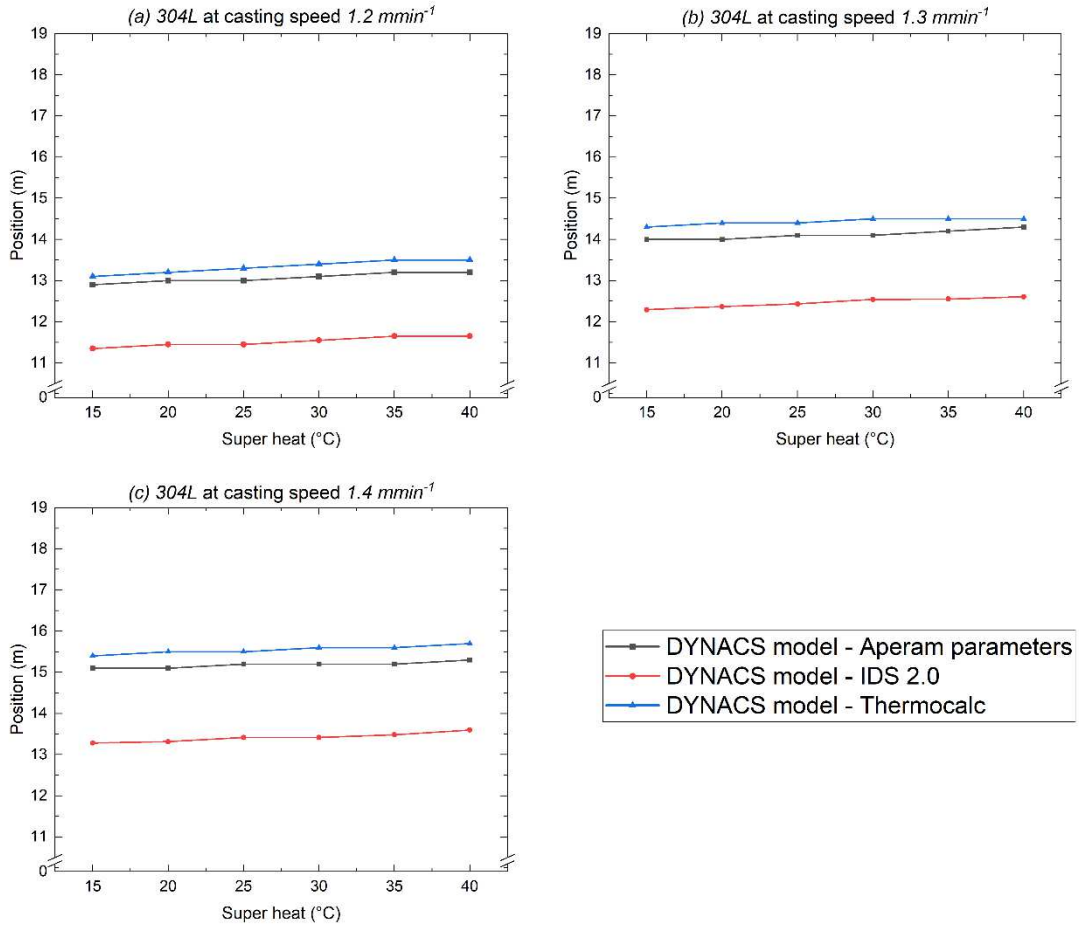

Figure 24: Solidification profile obtained from the DYNACS model for the steel grade 304L; (a) 1.2 mmin^{-1}, (b) 1.3 mmin^{-1} (c) 1.4 mmin^{-1}

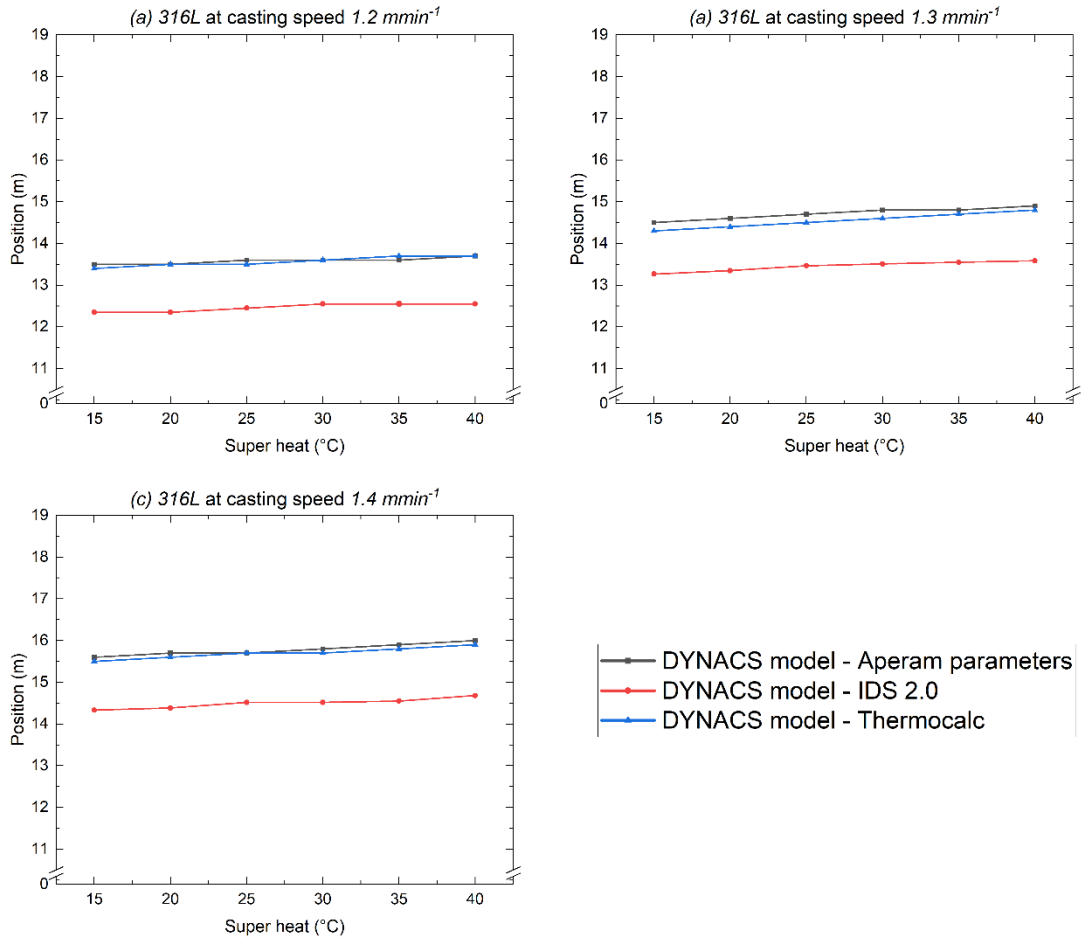

Figure 25: Solidification profile obtained from the DYNACS model for the steel grade 316L; (a) 1.2 mmin^{-1}, (b) 1.3 mmin^{-1} (c) 1.4 mmin^{-1}

The primary goal was to assess the consistency and accuracy of the predicted solidification points for each parameter set (Aperam, Thermo-Calc, and IDS 2.0) in the DYNACS model. The overall caster length is 24 m in the Aperam – plant. The steel needs to be fully solidified before leaving the caster. The predicted solidification points along the caster length showed a high level of coherence among the three parameters sets. Especially, IDS 2.0 parameters give lower solidification points in the predictions, while Thermo-Calc and Aperam parameters give higher solidification points and lie close to each other. These variations might be attributed to the variation in the thermophysical parameters values used in the model.

A comparison of steel grades 304L and 316L indicates that the grade 316L has a higher solidification point for all three parameter sets. The observed difference in the solidification behavior could be the presence of additional alloying elements in 316L such as higher molybdenum and nickel content. Steel 316L has higher molybdenum and nickel content that can result in stabilization of austenite at lower temperatures. Both molybdenum and nickel are austenite stabilizers, promoting the formation of austenite

during solidification [Figure 26]. Austenite, with its higher solidification temperature as compared to other phases, can cause a delay in the transformation to the lower temperature phases, resulting in extended solidification time [55].

The lower chromium content in steel 316L also influences the solidification behavior. Chromium is a ferrite stabilizer and assists in the formation of delta ferrite, that solidifies at lower temperature as compared to austenite. Lower chromium content can result in limited delta ferrite formation and the transformation to delta ferrite occurs late, resulting in delayed solidification [Figure 26]. Similarly, lower manganese content in steel 316L can slow down the phase transformation process. The steel will stay in liquid state for an extended duration before complete solidification, resulting in delayed solidification [56].

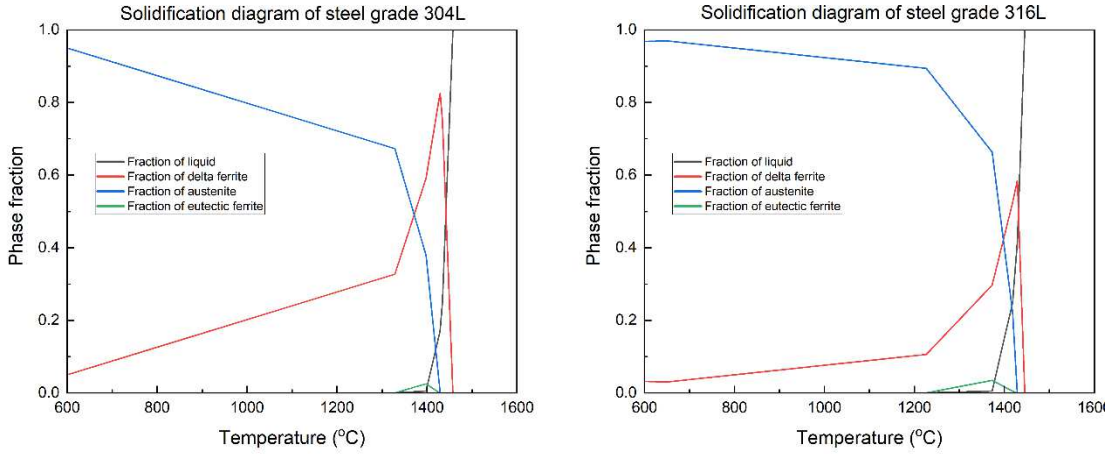

Figure 26: Solidification diagram of steel grades 304L and 316L – IDS calculations

However, it is crucial to consider the solid – solid transformations, such as the transformation from austenite to ferrite or bainite, that occur after the liquid phase has solidified. These transitions do not have any effect on the overall solidification time or temperature, thus have no effect on the solidification process.

4.3 CFD model of the continuous casting process

In this section, we present the analysis of the temperature and solidification behavior from the two-dimensional heat transfer and solidification model using ANSYS – Fluent. The simulations were performed using the industrial steel grades and industrial plant casting conditions so that the results could be compared with these of the DYNACS model. The core of this section lies in assessing the influence of the different thermophysical parameters and how the temperature and solidification profiles change with using different sets of thermophysical parameters.

4.3.1 Temperature profile

In continuous casting, the temperature distribution directly influences the solidification behavior and the overall product quality. Therefore, understanding and controlling the

temperature profiles is important in ensuring uniform solidification. In this section, the influence of different thermophysical parameters on the temperature profiles as predicted by CFD simulations are discussed. Also, the effect of different thermophysical parameters on the temperature distribution in different regions of the casting mold and secondary cooling regions are discussed. Different temperature contours are used to visualize the temperature distribution in the mold and the secondary cooling region, allowing us to identify the temperature change and the critical zones, highlighting the temporal evolution of temperature throughout the casting.

Figure *27* illustrates the temperature contour from the side angle for the mold and the secondary cooling region for steel grade 316L. It provides a comprehensive visual representation of the spatial temperature distribution, elaborating the thermal behavior during the process. As the liquid steel enters the mold region, the temperature is initially high, but once the steel enters the water-cooled mold walls, the temperature starts to decrease. The temperature gradually decreases further in the secondary cooling region, due to the interaction with the water sprays. We see a pronounced shift in temperature from inlet position till the end of casting, reflecting the combined effect of heat extraction and solidification.

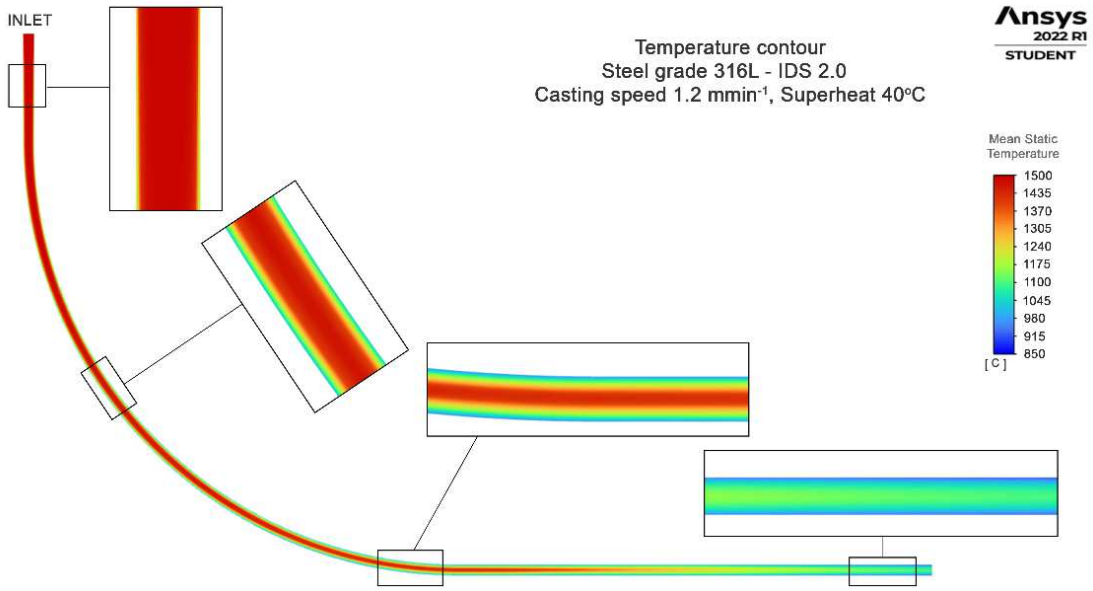

Figure 27: Temperature contour of the mold and secondary cooling region for steel grade 316L by using IDS 2.0 parameters, at casting speed 1.2 mmin^{-1}, superheat 40 °C.

The heat transfer directly depends on the thermophysical parameters of the steel and the process conditions of the casting. To understand the effect of the thermophysical parameters on the heat transfer, the process conditions are kept the same for all the simulations, whereas the thermophysical parameter values are varied between the three sets Aperam, IDS 2.0 and Thermo-Calc. Figure *28* shows the plotted temperature contours for zone 7 and zone 8 of the secondary cooling region for the steel grade 304L. The Thermo-Calc parameter set shows a gradual heat extraction, as seen by the

difference in temperature of the outer wall and the inner temperature. The Aperam parameter set has a relatively higher value of thermal conductivity, able to rapidly conduct heat away from the steel. It gives a more uniform temperature distribution in the outer and inner surface at the end.

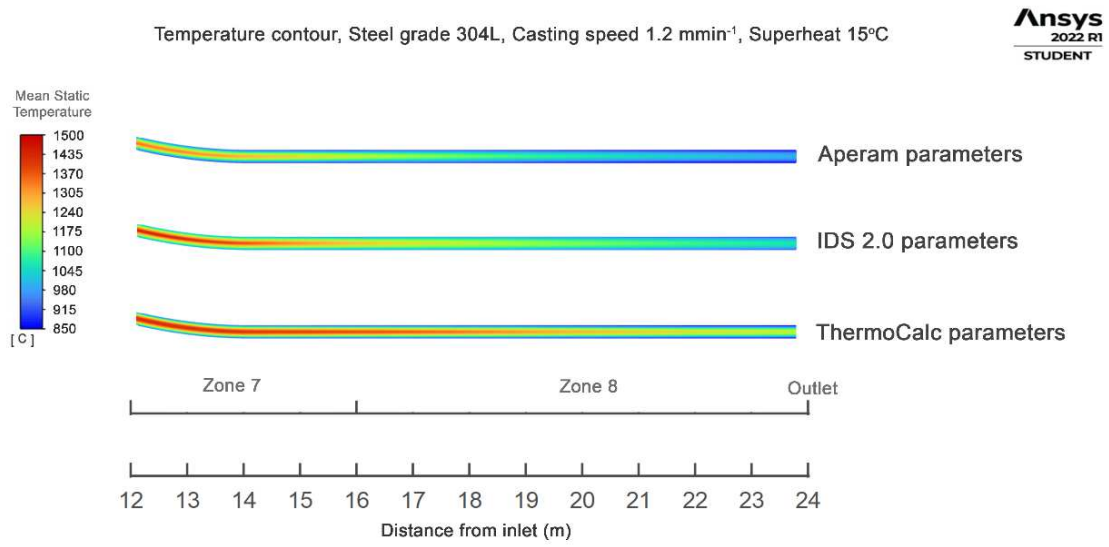

Figure 28: Temperature contours of the secondary cooling region for the steel grade 304L, at casting speed 1.2 mmin^{-1}, superheat 15 °C

Figure 29 and Figure 30 show the obtained temperature values in zone 7 at the location of the pyrometer for the different sets of thermophysical parameters for respectively steel grades 304L and 316L.

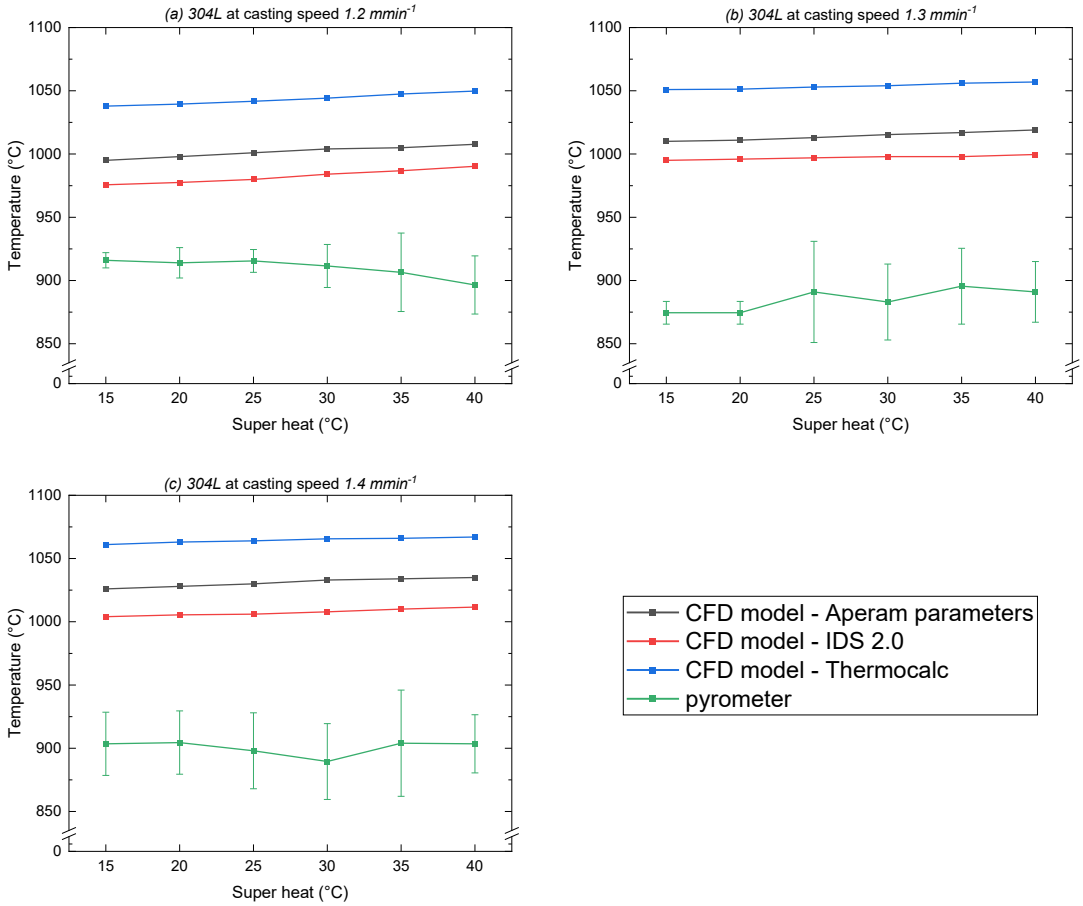

Figure 29: Temperature distribution at zone 7 obtained from the CFD model for the steel grade 304L; (a) 1.2 mmin^{-1}, (b) 1.3 mmin^{-1} (c) 1.4 mmin^{-1}

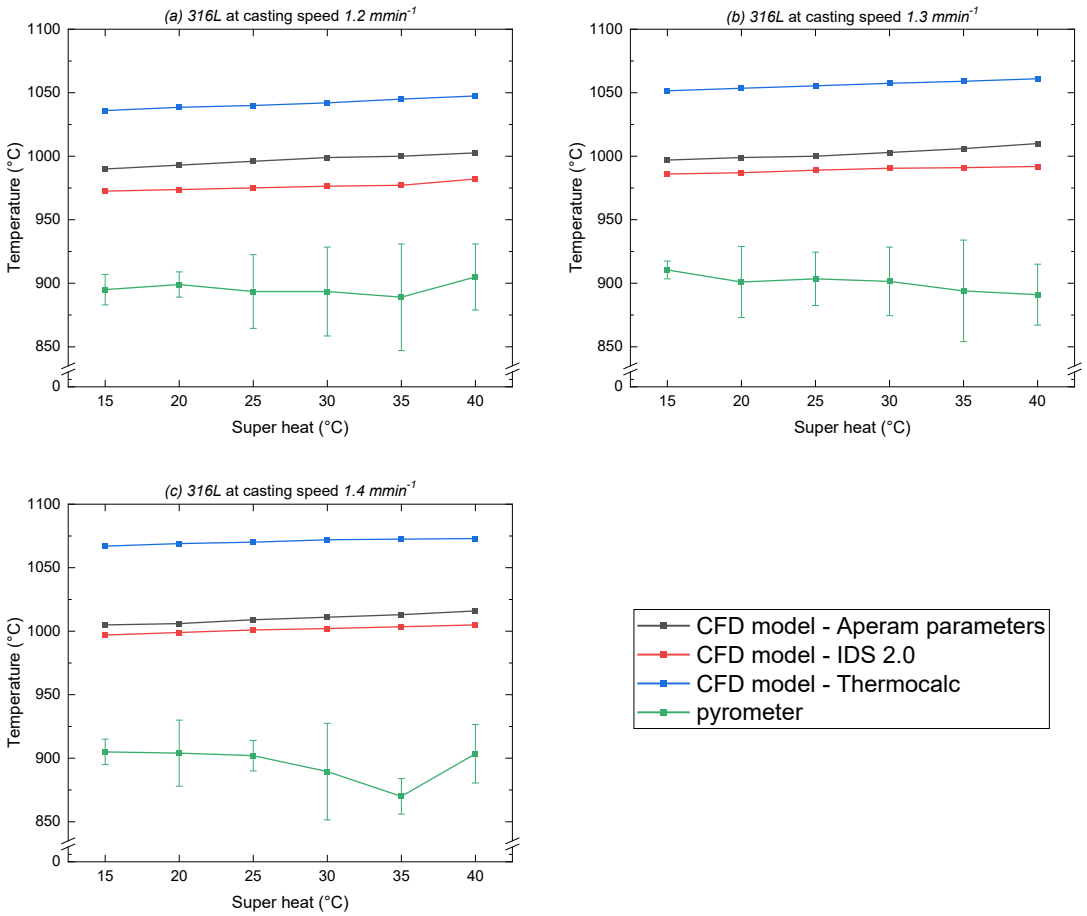

Figure 30: Temperature distribution at zone 7 obtained from the CFD model for the steel grade 316L; (a) 1.2 mmin^{-1}, (b) 1.3 mmin^{-1} (c) 1.4 mmin^{-1}

In the previous section 4.2.1, the temperature results of the DYNACS model were thoroughly discussed, showing a notable consistency in the temperature values with small variations. However, the current results demonstrate that the predicted temperature values with the CFD model for all parameter sets (Aperam, Thermo-Calc, and IDS 2.0) exhibit variations at zone 7 for both 304L and 316L, exhibiting a similar trend to the DYNACS model. Despite this resemblance, distinct peculiarities exist for temperature results in the CFD model. The temperature values with the CFD model appear to be more dispersed than those of the DYNACS model. Also, the temperature values with the Thermo-Calc parameters are significantly higher than with the Aperam and IDS 2.0 parameters. These observed peculiarities suggest that the two models use different approaches to account for specific heat and mass transfer phenomenon. The DYNACS model's close temperature ranges could indicate that its calculations are driven by heat transfer equations using a special integral method, as indicated in the model description. This method contributes to the model's ability to produce accurate and reliable temperature predictions. On the other hand, the CFD model's wide temperature range could indicate that its calculations are based on a more complex framework, using

the Navier-Stokes equations and the turbulent k - ε model to capture a broader heat and mass transfer phenomenon.

4.3.2 Solidification profile

The solidification process is the critical step of continuous casting, as it directly impacts the quality of the final steel product. Understanding the solidification behavior is very important in optimizing the continuous casting process and ensuring production efficiency. The key aspect of this study is to simulate different liquid fraction contours for different sets of thermophysical parameters to understand how the liquid fraction changes during the casting. Liquid fraction contours help in better visualizing the solidification point where steel is completely solidified, ensuring the steel is solidified before exiting the last zone.

Figure *31* illustrates the liquid and solid fraction in the mold and the secondary cooling region for 316L steel grade. This helps in visually analyzing the liquid fraction in the molten steel and its transformation into the solidified shell in any region. As the molten steel enters the mold region, it is completely liquid, shown by warmer color in the contour plot. The mold walls are water cooled which allows the formation of a solidified shell along the walls. As the steel passes through the water spray secondary cooling regions, the solid fraction gradually increases along the walls while the center of the slab is still in liquid state. The contours show the gradual formation of the solidification front from the mold wall to the strand's center, showing the solidification process over time. Furthermore, the liquid fraction contours help in identifying the critical areas of non-uniform cooling, to further improve the uniformity of the casting process.

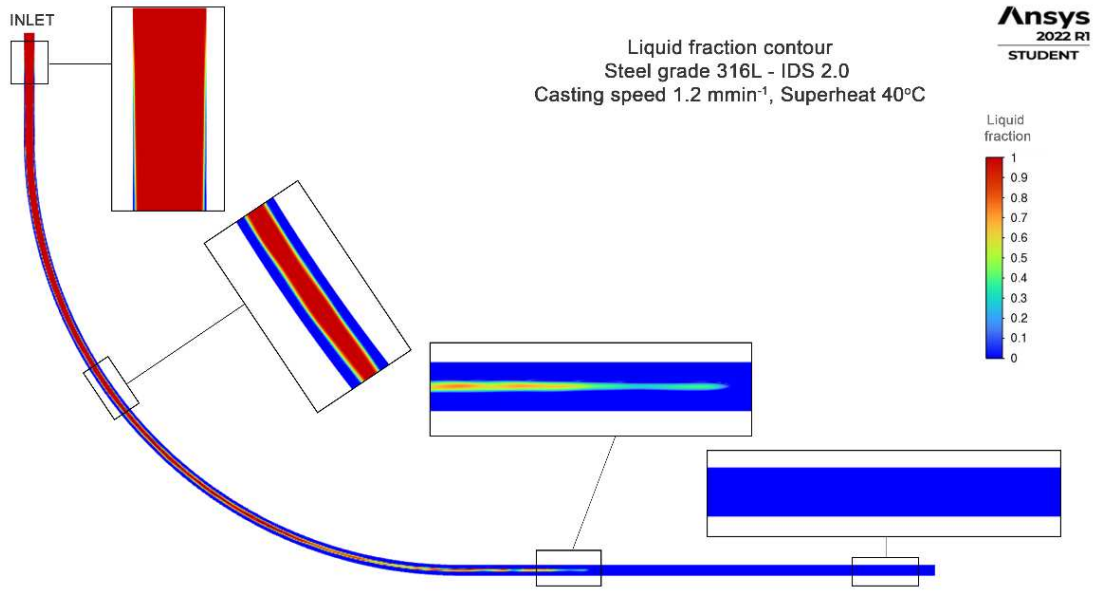

Figure 31: Liquid fraction contour of the steel grade 316L by using IDS 2.0 parameters, at casting speed 1.2 mmin^{-1}, superheat 40 °C.

Figure 32 shows the plotted liquid fraction contours for the mold region by using the different sets of thermophysical parameters for 304L steel grade and keeping the same process conditions. We can interpret from the different contour plots how the difference in thermophysical parameters affects the cooling and solidification behavior. These contours illustrate how the molten steel starts to solidify from the walls of the mold region. The solidification with the Thermo-Calc parameter set starts a bit later than for the other parameter sets, which can be the result of the higher liquidus temperature and lower thermal conductivity in the Thermo-Calc set.

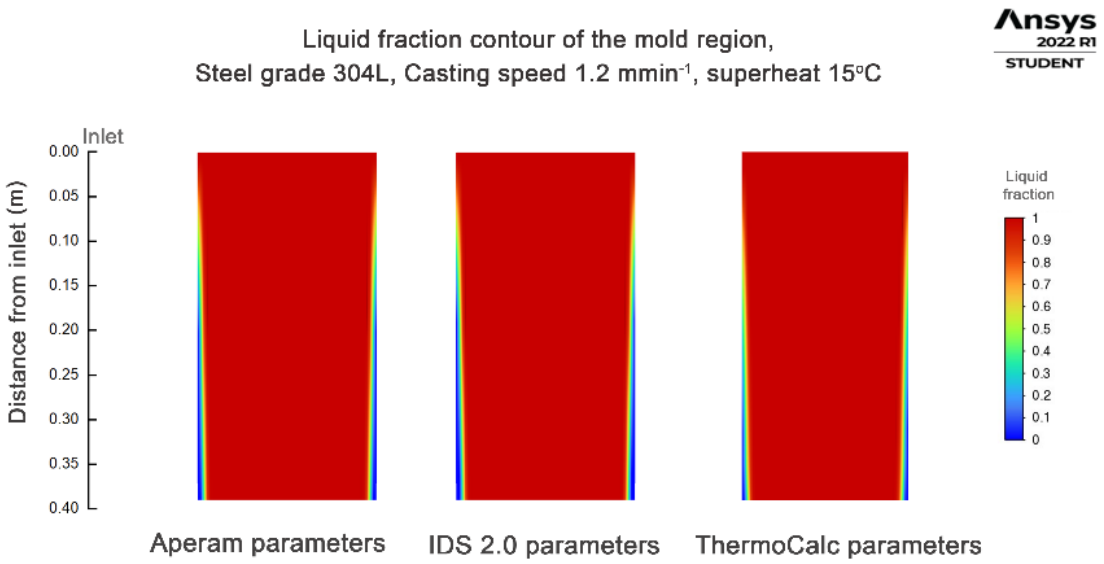

Figure 32: Liquid fraction contours of the mold region of different sets of thermophysical parameters for the steel grade 304L, at casting speed 1.2 mmin-1, superheat 15 °C

Figure 33 and *Figure* 34 show different solidification points by using the different sets of the thermophysical parameters and keeping the same boundary conditions. The difference in the results highlights the significant impact of these parameters on the solidification process, which is critical for the casting process.

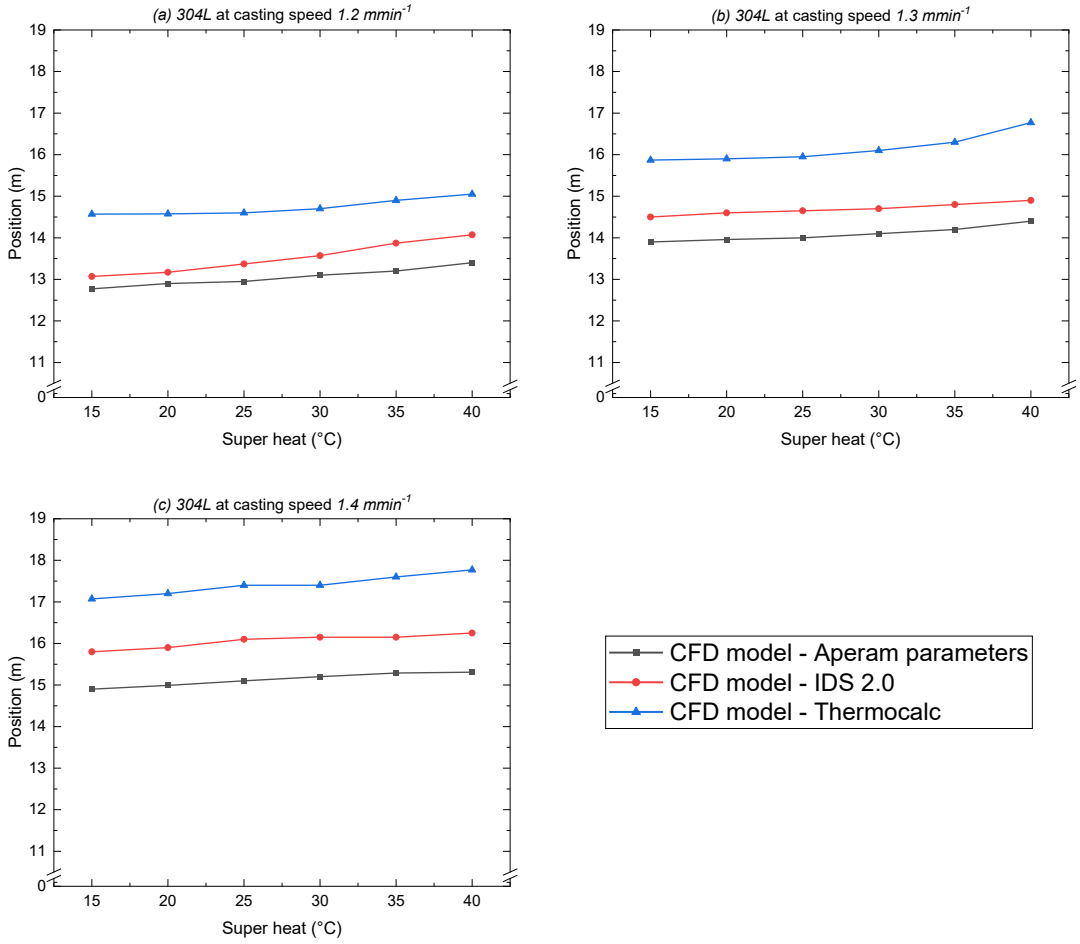

Figure 33: Solidification profile obtained from the CFD model for the steel grade 304L; (a) 1.2 mmin^{-1}, (b) 1.3 mmin^{-1} (c) 1.4 mmin^{-1}

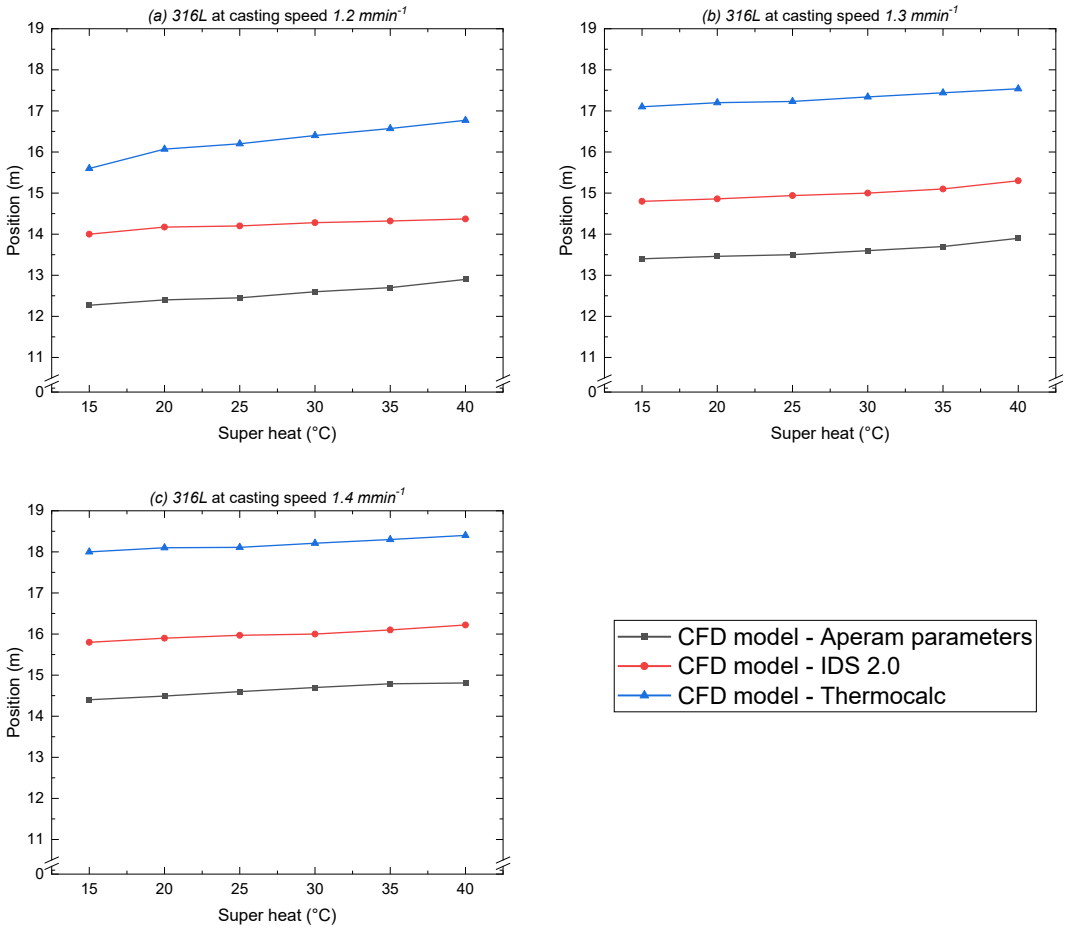

Figure 34: Solidification profile obtained from the CFD model for the steel grade 316L; (a) 1.2 mmin^{-1}, (b) 1.3 mmin^{-1} (c) 1.4 mmin^{-1}

In the previous section 4.2.2, the solidification results of the DYNACS model were thoroughly discussed, showing close proximities with small variations in the solidification points for all parameter sets (Aperam, Thermo-Calc, and IDS 2.0) for both steel grades 304L and 316L: IDS 2.0 parameters showed the lowest solidification points, followed by the Aperam and Thermo-Calc parameters with a minimal difference between them. However, the current results focus on the predicted solidification points with the CFD model showing a more dispersed range of solidification points. In the CFD model, the Aperam parameters showed the lowest solidification points, followed by the IDS 2.0 parameters, which was moderately higher, and then Thermo-Calc parameters showed relatively higher solidification points.

The difference in the solidification profiles between the DYNACS model and the CFD model can be due to various factors related to the numerical formulations and the assumptions about the heat and mass transfer phenomenon during solidification. The DYNACS model calculates the solidification point based on the DYNASHELL shell thickness correlation (Eq. 8) while CFD model calculates the solidification point using the

Navier-Stokes equations and incorporating a turbulent k - ε model, which may lead to different interpretations of the solidification points.

4.4 Parametric influence on temperature and solidification profile

It is very important to understand the influence of the different thermophysical parameters on the behavior of the different steel grades during solidification. In this section, the term "parametric influence" refers to the effective research into how changes in individual parameters, such as the solidus and liquidus temperature, the density, the thermal conductivity, the specific heat, and the latent heat, affect the overall temperature distribution and the solidification profile. For this study, every single parameter of IDS 2.0 is altered within the Aperam set of thermophysical parameters for the steel grades 304L and 316L. Through the CFD model, the primary influence of each parameter is investigated by keeping all other parameters constant and altering them one at a time under the same process conditions. This approach not only clarifies the roles of the individual parameters, but it also helps to predict the behavior of the steel grade under varying processing conditions such as the casting speed and the superheat.

4.4.1 Temperature profile

Figure 35 and *Figure* 36 show the parametric influence in terms of temperature at zone 7 of secondary cooling by altering a single parameter in the Aperam parameter set in comparison to the default Aperam set and the IDS 2.0 parameter set by using the CFD model for steel grades 304L and 316L.

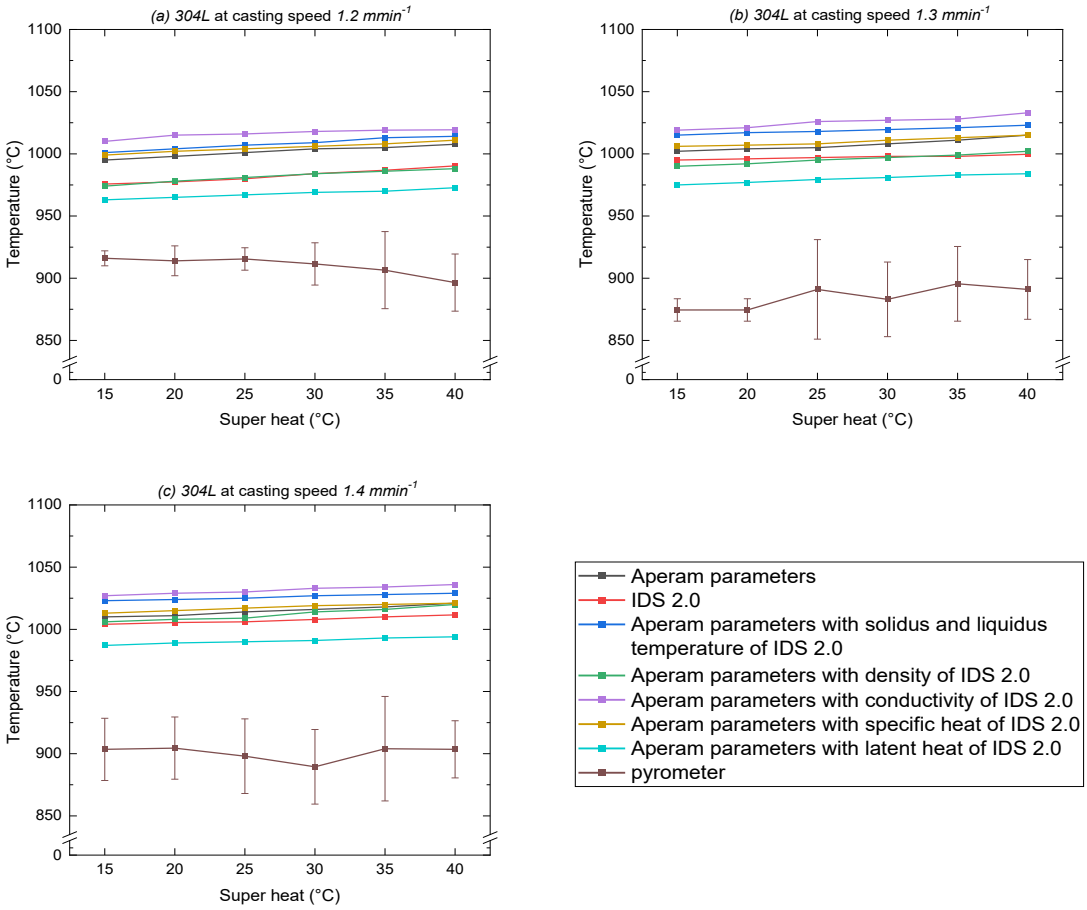

Figure 35: Temperature distribution at zone 7 obtained from the CFD model for the steel grade 304L by varying different parameters; (a) 1.2 mmin^{-1}, (b) 1.3 mmin^{-1} (c) 1.4 mmin^{-1}

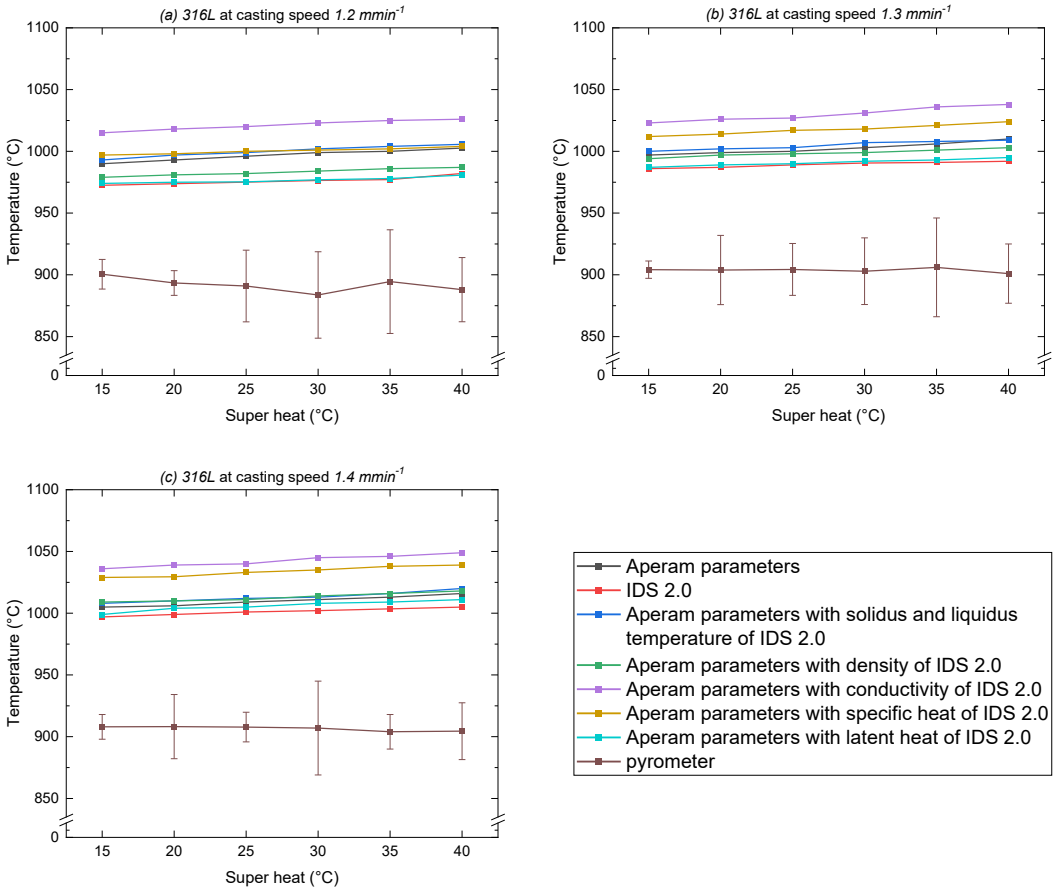

Figure 36: Temperature distribution at zone 7 obtained from the CFD model for the steel grade 316L by varying different parameters; (a) 1.2 mmin^{-1}, (b) 1.3 mmin^{-1} (c) 1.4 mmin^{-1}

Solidus and liquidus temperature:

The solidus and liquidus temperatures are crucial for predicting the solidification behavior of steel. These temperatures act as boundary points and govern phase transitions within the temperature profile of steel. Modifications to these temperatures can lead to alterations in the phase transitions, thereby effects the casting process, especially in scenarios demanding precise control over cooling.

The CFD simulations employed the higher solidus and liquidus temperatures of IDS 2.0, resulted in a 10 – 15 °C increase in the temperature of zone 7 across all three casting speeds, suggesting that the phase transition occurs at higher temperatures. The observed temperature increase with the higher phase transition values highlights the critical role these temperatures play in determining the final solidification temperature of the steel.

Density:

The steel density has a significant impact on the temperature profile, as it is linked with the heat energy steel stores per unit volume. Steel with a high-density value can store more heat energy, resulting in a more stable temperature distribution. As a result, a high-density steel shows a more gradual temperature change due to the slower absorption and release of heat energy. Furthermore, a high density steel inherently allows slower heat transfer from the liquid too the surrounding environment, resulting in longer transition times and a slower rate of temperature change. As a result, variations in density have a direct impact on the heat conduction behavior within the material, leading to observable disparities in the temperature values.

The CFD simulations employed lower liquid density values of IDS 2.0, while keeping all other thermophysical parameters of the Aperam set for steel grades 304L and 316L, resulted in a 10 – 25 °C decrease in the temperature of zone 7 across all three casting speeds. This facilitates faster heat transfer from the liquid to the surrounding environment, potentially accelerating the cooling rate.

Thermal conductivity:

Thermal conductivity is very important in determining how effectively heat is transferred from one region to another. Heat conduction is more efficient in steel with higher thermal conductivity values, which results in a more uniform temperature distribution during the casting. Heat can quickly flow from higher-temperature regions to lower-temperature regions, limiting the formation of localized hotspots. On the other hand, steels with a lower thermal conductivity exhibit a lower heat conduction rate, resulting in slower temperature change. So, the change in the thermal conductivity values can strongly affect the heat conduction behavior of the steel in the model, which ultimately produces observable variations in the temperature distribution.

The CFD simulations employed lower thermal conductivity values of IDS 2.0, while keeping all other thermophysical parameters of the Aperam set for steel grades 304L and 316L, resulted in ~ 25 °C increase in the temperature of zone 7 across all three casting speeds. This outcome is attributable to slower heat transfer rate and the ensuing heat accumulation within the steel.

Specific heat:

Specific heat plays a pivotal role in determining the temperature profile of a steel grade since it directly influences the rate at which the temperature of a steel changes. Steels with higher specific heat can retain more thermal energy per unit mass and resist change in temperature. This characteristic is important during phase transformations, such as solidification, where the absorption or release of latent heat can influence the temperature profile.

The CFD simulations employed higher specific heat values of IDS 2.0, while keeping all other thermophysical parameters of the Aperam set for steel grades 304L and 316L, resulted in ~ 5 °C increase in the temperature of zone 7 across all three casting speeds. The slight change in temperature explains the steel ability to store more energy during

solidification, highlighting the importance of considering material properties in continuous casting simulations.

Latent heat:

Latent heat is directly linked with the temperature profile of the steel, particularly during the phase change. It is defined as the energy absorbed or released by the steel during phase transition, without changing the temperature. During the phase change from the liquid state to the solid state, latent heat is released, resulting in the formation of a temperature plateau that remains constant for a period. The stability of temperature is a direct result of the latent heat being used for the phase transition, instead of being reflected in the steel as a temperature change. Changing the latent heat value directly influences the temperature stabilization period.

The CFD simulations employ lower latent heat of IDS 2.0, while keeping all other thermophysical parameters of the Aperam set for steel grades 304L and 316L, resulted in 15 - 25 °C decrease in the temperature of zone 7 across all three casting speeds. This is because the lower latent heat requires less energy for phase change leading to a shorter plateau in the temperature profile. After a shorter period of stabilization, the temperature decreases more rapidly, resulting in the observed temperature drop.

4.4.2 Solidification profile

Figure 37 and *Figure* 38 show the parametric influence in term of the solidification profile by altering a single parameter in the Aperam parameter set in comparison to the default Aperam set and the IDS 2.0 parameter set by using CFD model for steel grades 304L and 316L.

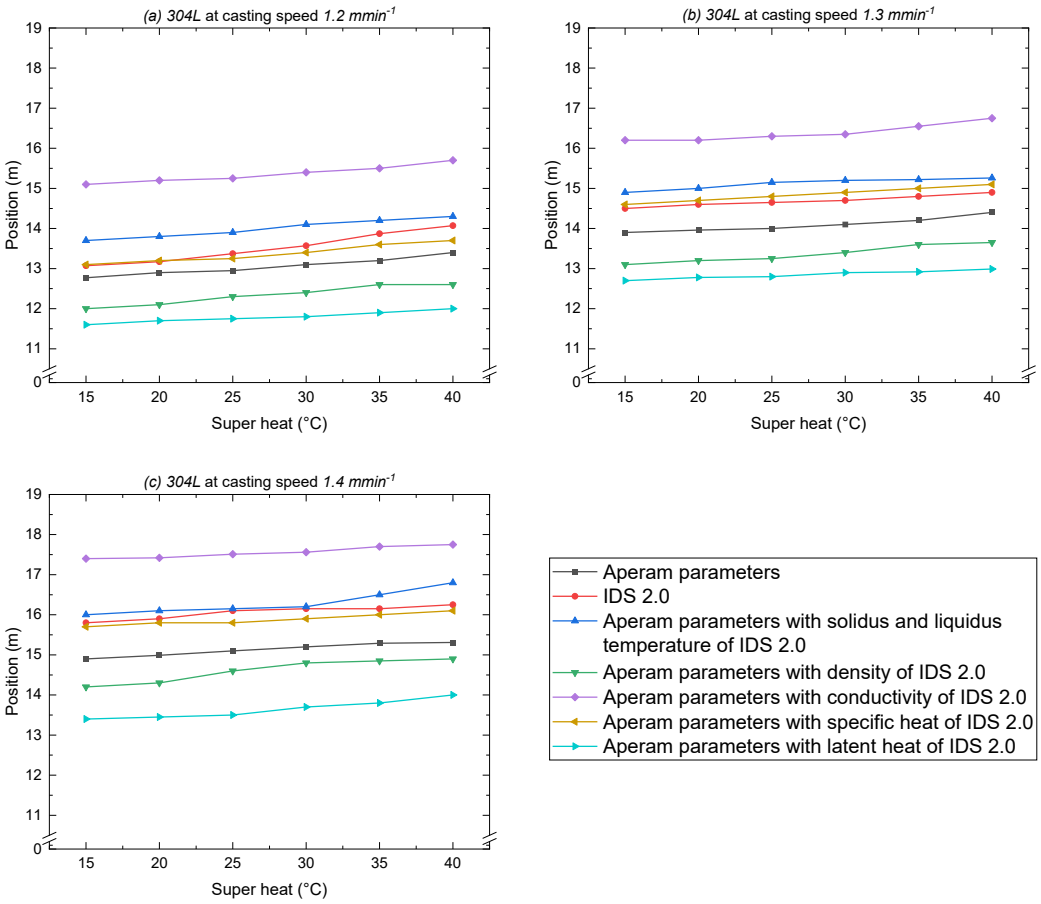

Figure 37: Solidification profile obtained from the CFD model for steel grade 304L by varying different parameters; (a) 1.2 mmin^{-1}, (b) 1.3 mmin^{-1} (c) 1.4 mmin^{-1}.

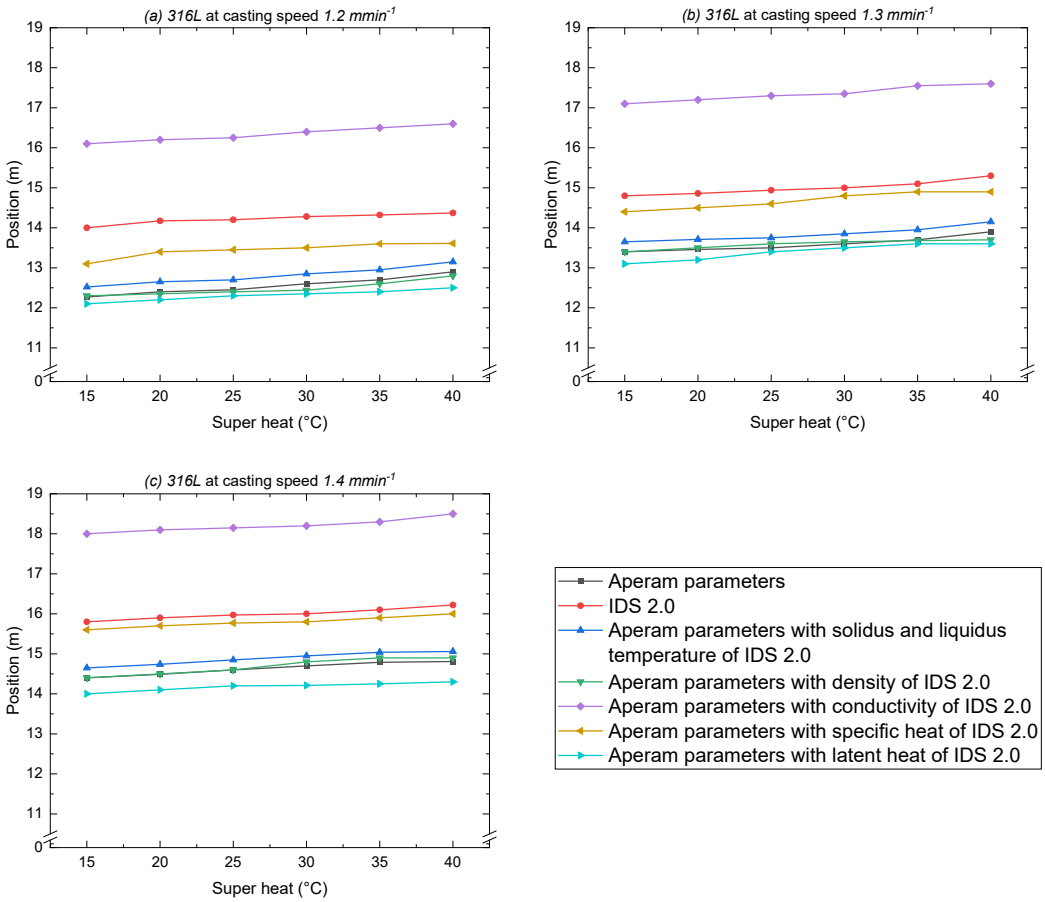

Figure 38: Solidification profile obtained from the CFD model for steel grade 316L by varying different parameters; (a) 1.2 mmin^{-1}, (b) 1.3 mmin^{-1} (c) 1.4 mmin^{-1}.

Solidus and liquidus temperature:

The CFD simulations employed the higher solidus and liquidus temperatures of IDS 2.0, resulted in 0.5 – 1 m delayed onset of solidification across all three casting speeds because the temperature must reach a higher value before solidification starts. As the steel undergoes cooling, it maintains a liquid or semi-liquid state for a shorter duration and requires a higher temperature than previously needed for complete solidification. This gives a direct relationship between the phase transition temperatures and the point on the strand at which the solidification ends.

Density:

Density plays a crucial role in the solidification profile, influencing buoyancy–driven flows in the mushy state, which can affect the solidification range, particularly in case of natural convection.

The CFD simulations employed the lower liquid density values of IDS 2.0, while keeping all other thermophysical parameters of the Aperam set for steel grades 304L and 316L,

resulted in ~ 0.5 m earlier onset of solidification across all three casting speeds. It facilitates more efficient heat transfer, resulting in an accelerated solidification process and reaching the solidification point earlier.

Thermal conductivity:

The CFD simulations employed lower thermal conductivity values of IDS 2.0, while keeping all other thermophysical parameters of the Aperam set for steel grades 304L and 316L, resulted in 3 – 3.5 m delayed onset of solidification across all three casting speeds. This is attributable to the slower heat dissipation rate within the steel as the heat generated during the solidification is not properly transferred away from the solidifying front to its surrounding environment, leading to a delayed onset of the solidification point, as observed.

Specific heat:

The CFD simulations employed higher specific heat values of IDS 2.0, while keeping all other thermophysical parameters of the Aperam set for steel grades 304L and 316L, resulted in 0.5 – 1 m delayed onset of solidification across all three casting speeds. This is attributable to the more energy requirement for phase transitions from liquid to solid. The steel retains its thermal energy for a longer duration, which results in a noticeable delay in the initiation of the solidification point, as observed.

Latent heat:

The CFD simulations employed lower latent heat of IDS 2.0, while keeping all other thermophysical parameters of the Aperam set for steel grades 304L and 316L, resulted in 1.5 – 2 m earlier onset of solidification across all three casting speeds. It is attributed to the lower energy requirements for phase transition from liquid to solid phase, resulting in a narrower and faster solidification plateau.

Throughout this study, it has become evident that changing specific parameters has a significant impact on the temperature profile and the solidification profile of the steel. Whether it is adjusting the solidus and liquidus temperatures, the thermal conductivity, the specific heat or other thermophysical properties, each change introduces a distinctive heat transfer behavior, that is important in understanding the steel response during the casting process. However, the most significant variations in temperature and solidification profile were observed when the thermal conductivity values were altered compared to the other parameters.

4.5 Optimized parameter analysis – the influence of thermal conductivity

The results of the parametric study showed that the thermal conductivity values have the most significant influence on the temperature and solidification profile [Section 4.4]. The IDS 2.0 parameters have a lower thermal conductivity as compared to the Aperam parameters. This section analyses the impact of thermal conductivity by employing the Aperam's thermal conductivity value in conjunction with all other IDS parameters, and

vice versa, using the IDS's thermal conductivity value with all other Aperam parameters to explain the critical role of thermal conductivity.

4.5.1 Temperature profile

The parametric study shows that the variation in the thermal conductivity can strongly affect the heat conduction behavior of the steel in the model, which ultimately results in an observable change in temperature profile. When the lower thermal conductivity value of IDS 2.0 is used with all other parameters of the Aperam set for both steel grades 304L and 316L, the reduced heat dissipation results in elevated temperatures. This suggests that the thermal conductivity of the Aperam parameter set, when used with all other IDS 2.0 parameters, would result in a more effective heat dissipation. This leads to a lower temperature profile as shown in Figure *39*.

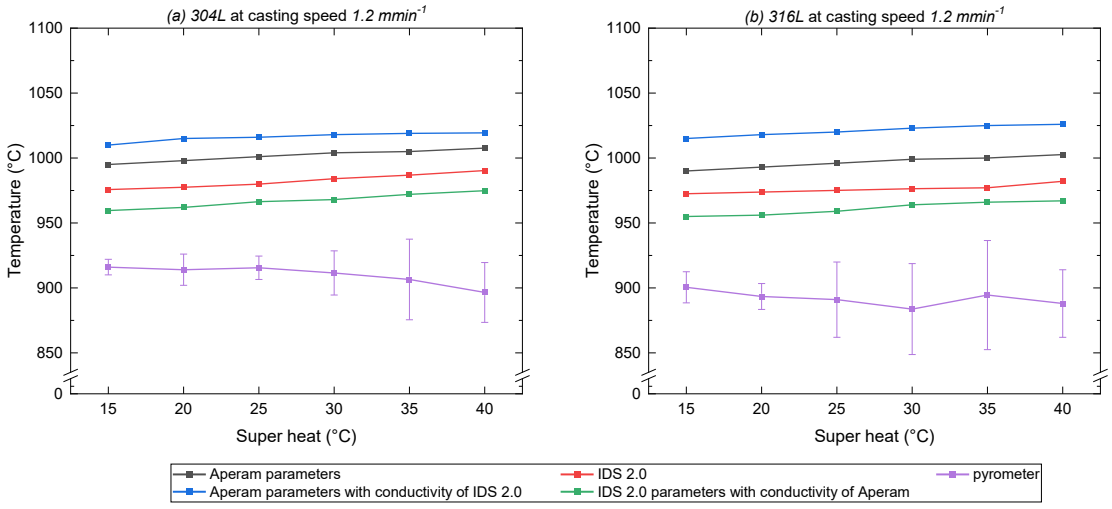

Figure 39: Comparative analysis of temperature distribution at zone 7 obtained from the CFD model for the Aperam and IDS parameters when thermal conductivity values are exchanged; (a) Steel grade 304L, (b) Steel grade 316L.

4.5.2 Solidification profile

The parametric study highlights the significant importance of thermal conductivity on the solidification profile. When a lower thermal conductivity value of IDS 2.0 is used with all other parameters of Aperam for both steel grades 304L and 316L, solidification occurs at a very delayed rate. This suggests that when the thermal conductivity of the Aperam parameter set is used in conjunction with all other IDS 2.0 parameters, the cooling

process accelerates significantly, leading to an earlier transition from the liquid to the solid phase as shown in Figure *40*.

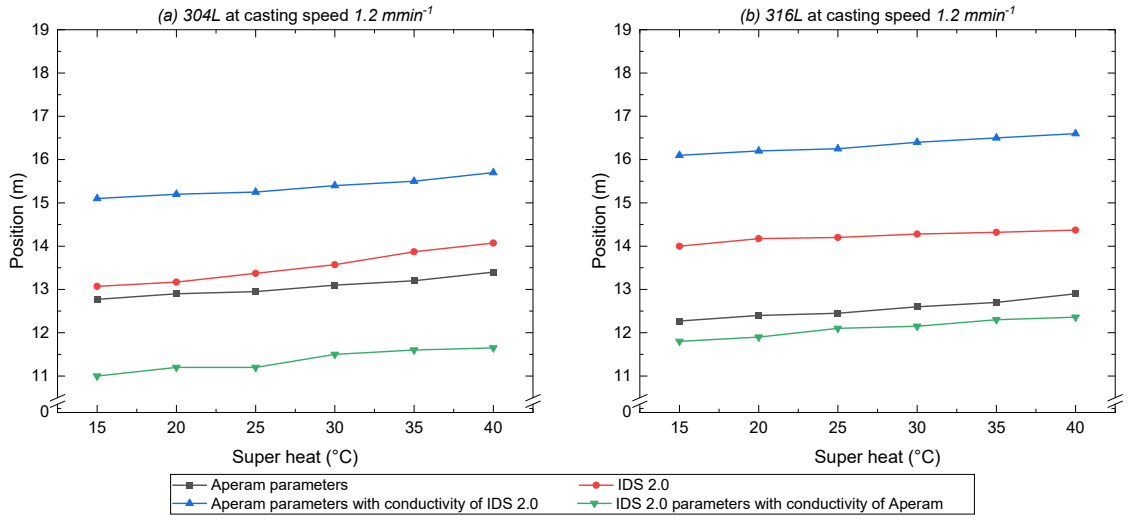

Figure 40: Comparative analysis of the solidification profile obtained from the CFD model for the Aperam and IDS parameters when thermal conductivity values are exchanged; (a) Steel grade 304L, (b) Steel grade 316L.

The analysis of the influence of varying the thermal conductivity on the steel grade 304L and 316L shows that swapping their conductivities has a considerable impact on the temperature and the solidification profile. The notable effect of thermal conductivity signifies its crucial role in optimizing the parameters and offers foundations for further research in the temperature and solidification studies.

Chapter 5: Conclusion and future perspectives

5.1 Conclusion

This study aimed to investigate and understand the solidification behavior of molten steel during the casting process and evaluate the accuracy of the DYNACS model for two steel grades, 304L and 316L. For this purpose, we collected a comprehensive set of thermophysical parameters, including solidus and liquidus temperatures, density, thermal conductivity, specific heat, and latent heat, for both steel grades. Additionally, we calculated the essential thermodynamic inputs, specifically heat transfer coefficient (HTC) for the mold and secondary cooling region for model development. By employing these data, we investigated how the thermophysical parameters influence the outcomes of both the industrial DYNACS and CFD models. The model predictions are also compared with the real temperature data obtained from a pyrometer at the continuous caster.

The findings of this study demonstrate the critical importance of these inputs by implementing different set of thermophysical parameters (Thermo-Calc, IDS, and Aperam) and different HTC for the mold and the secondary cooling region. It became evident that these thermophysical and thermodynamic inputs are interconnected components of a complex system. Change in one parameter can have an impact on the entire process, influencing the temperature and solidification profile at the continuous caster. The main conclusions of this work were the following:

- The comparison of results from Thermo-Calc, IDS, and Aperam values reveals significant variations in the values of the thermophysical parameters for steel grades 304L and 316L. Thermo-Calc consistently yields higher values for solidus and liquidus temperatures and specific heat, while IDS data bridges the gap between Aperam and Thermo-Calc values. These differences are attributed to the distinct thermodynamic databases, mathematical models, and phase diagrams used by each tool, highlighting the sensitivity of thermophysical parameter values to modeling choices.
- The temperature and solidification predictions obtained from the DYNACS model for all three parameter sets (Aperam, Thermo-Calc and IDS 2.0) were found to be closely aligned, with the IDS 2.0 parameters predicted lower temperatures and solidification points, with the Thermo-Calc and Aperam parameters produce slightly higher values.

These variations are attributed to the differences in the thermophysical properties associated with each parameter set.

- While comparing steel grades 304L and 316L in the DYNACS model predictions, steel grade 304L consistently has higher temperature values, whereas steel grade 316L has higher solidification points across all three parameter sets. These differences are attributed to alloy composition differences, specifically the higher molybdenum content in 316L, which influences phase transformation kinetics, heat dissipation, and solidification behavior. The DYNACS model is sensitive to minor parameter variations, but the overall impact is relatively small. Careful parameter selection is still important for accurate predictions.
- The temperature and solidification predictions obtained from the CFD model show distinct characteristics compared to the DYNACS model. Temperature values in the CFD model have a wider dispersion and significantly higher values for Thermo-Calc parameters, indicating the difference in the approach to modeling specific heat and mass transfer phenomena. In terms of solidification, the CFD model predicts a more dispersed range of solidification points, with Aperam parameters predicting the lowest, followed by IDS parameters and Thermo-Calc parameters, considering differences in numerical formulations and assumptions concerning heat and mass transfer during solidification.
- A comparison of the CFD model and the DYNACS model reveals significant differences in temperature and solidification predictions. While both models provide valuable insights, the CFD model, which is driven by the Navier-Stokes equations and incorporates a turbulent k-ε model, has wider temperature ranges and more dispersed solidification points compared to the DYNACS model. These variations highlight the importance of the numerical formulations and underlying assumptions used in each model, highlighting the importance of thermodynamic inputs and modelling approaches in continuous caster simulations.
- The predictions of Aperam and IDS parameters are relatively closer to real temperature pyrometer values, allowing us to consider every individual parameter of IDS and implement in the Aperam parameter to evaluate the parametric influence on both temperature and solidification profiles. These findings highlight the critical role of specific thermophysical parameters in predicting both temperature and solidification profiles, providing an essential insight for industrial casting processes.
- The CFD model showed the significant effect of parameter changes by varying individual parameters from IDS in comparison to Aperam set for steel grades 304L and 316L. The CFD model demonstrated that the solidus and liquidus temperatures, density, thermal conductivity, and latent heat had a major influence on the temperature and solidification profiles of steel, particularly the timing and extent of phase transitions, heat transfer efficiency, and temperature stabilization.
- The parametric study highlighted the importance of thermal conductivity on temperature and solidification profiles. When a lower thermal conductivity value of IDS 2.0 is used in conjunction with Aperam parameters, the results showed elevated temperatures and delayed solidification. Conversely, using Aperam's higher thermal conductivity values in conjunction with IDS parameters resulted in more effective heat dissipation and accelerated solidification. These findings highlight the important

role of thermal conductivity in parameters optimization, providing valuable insights for heat transfer and solidification in steel grades 304L and 316L.

While this research has advanced in understanding the role of individual parameters, it has also highlighted some limitations. The models used in this study, while robust, are based on certain assumptions and simplifications. The actual steel manufacturing process is inherently complex, with numerous variables at its functions. These findings should thus be regarded as a significant step forward, but more research is required to refine and expand on these insights.

5.2 Future perspectives

This study sets the foundation for future research. The complex relationships between thermophysical parameters and model results provide opportunity for future research. Improving the model and expanding the scope of data collection can lead to more accurate predictions and a better understanding of the continuous casting process.

- Based on the findings from the parametric influence, future research can delve deeper into multivariable parameter selection. Instead of changing one parameter at a time, comprehensive selection trials can be designed to identify the thermophysical parameter combinations that produce the desirable heat transfer and solidification profile. This approach will highlight the intricate interplay between various thermophysical parameters, providing a comprehensive understanding of how they interrelate to affect the steel solidification process and help in determining more accurate parameters inputs for the heat transfer model.
- It is important to extend this research to real-time process control for practical applications. Different algorithms and control systems can be linked, that can control the process parameters such as casting speed and water flow rate in adaptation to changing conditions. This approach can assist in maintaining precise control over temperature and solidification profiles and enable more efficient and cost-effective steel production.

In closing, this research represents a significant contribution to the field of metallurgy and steel manufacturing. The ability to link thermophysical and thermodynamic inputs to model outcomes marks a critical advancement in optimizing industrial processes. As the industry continues to evolve, our work serves as a foundation upon which future innovations can be built, ultimately enhancing the efficiency and sustainability of steel production.

,

Bibliography

[1] Nazem Jalali, P., Analysis of Different Continuous Casting Practices Through Numerical Modelling, 2015.
[2] Thomas, B.G., On-line Detection of Quality Problems in Continuous Casting of Steel. In F. Kongoli, Thomas, B.G., & Sawamiphakdi K. (Eds.), Modeling, Control, and Optimization in Ferrous and Non-Ferrous Industry (pp. 29-45), 2003.
[3] Aperam Belgium, HSBC Aperam Genk steel plant,
[4] Conference Report - 4th European Continuous Casting Conference, Ironmaking & Steelmaking 30 (2003), 2, pp. 82–94.
[5] Thomas, B.G., Continuous Casting (Metalurgy) - Yearbook of Science and Technology (2004).
[6] Anameric, B. and Kawatra, S.K., DIRECT IRON SMELTING REDUCTION PROCESSES, Mineral Processing and Extractive Metallurgy Review 30 (2008), 1, pp. 1–51.
[7] Pascon, F., 2D1/2 Thermal-Mechanical Model of Continuous Casting of Steel Using Finite Element Method, Université de Liège, Belgique, 2002.
[8] Yurko, L. Zhang, A. Allanore, C. Wang, J.S. Spangenberger and R.E. Kirchain et al., EPD Congress 2014, John Wiley & Sons, 2014.
[9] McCauley, W.L. and Apelian, D., Viscosity Characteristics of Continuous Casting Mold Fluxes, Canadian Metallurgical Quarterly 20 (1981), 2, pp. 247–262.
[10] Hanao, M., Kawamoto, M. and Yamanaka, A., Growth of Solidified Shell Just below the Meniscus in Continuous Casting Mold, ISIJ Int. 49 (2009), 3, pp. 365–374.
[11] IRVING W R., Continuous casting of steel, The Institute of Material: 1 Carlton House Terrace, London., 1993.
[12] Isaev, D., Borovik, A. and Osipov, O., Technological requirements to the drive of horizontal type continuous casting machine withdrawal-roll, 2015 International Siberian Conference on Control and Communications (SIBCON) (2015).
[13] Mauder, T., Sandera, C. and Stetina, J., Optimal Control Algorithm for Continuous Casting Process by Using Fuzzy Logic, steel research int. 86 (2015), 7, pp. 785–798.
[14] Huitron, R.M. Lopez, P. Vuorinen, E. Jalali, P. Kärkkäinen, M. Identification of cracking issues and process improvements through plant monitoring and numerical modelling of secondary cooling during continuous casting of HSLA …, 2021.
[15] Campbell, J., Complete casting handbook: Metal casting processes, metallurgy, techniques and design / John Campbell, Elsevier Butterworth-Heinemann, Amsterdam, 2015.
[16] Koric, S., Efficient thermo-mechanical model for solidification processes and its applications in steel continuous casting, 2006.

[17] Vapalahti, S., Thomas, B.G., Louhenkilpi, S., Castillejos, A.H., Acosta, F.A., Hernández., C.A., Heat Transfer Modelling of Continuous Casting: Numerical Considerations, Laboratory Measurements and Plant Validation, 2007.
[18] Santos, C.A., Spim, J.A. and Garcia, A., Mathematical modelling, and optimization strategies (genetic algorithm and knowledge base) applied to the continuous casting of steel, Engineering Applications of Artificial Intelligence 16 (2003), 5-6, pp. 511–527.
[19] Stefanescu, D.M., Length-Scale in Solidification Analysis, in: D.M. Stefanescu (Ed.), Science and engineering of casting solidification, Third edition, Springer, Cham, 2015, pp. 1–5.
[20] Vynnycky, M., Saleem, S., Devine, K.M., Florio, B.J., Mitchell, S.L., and O'Brien, S.B.G., On the formation of fold-type oscillation marks in the continuous casting of steel, Royal Society open science 4 (2017), 6, pp. 170062.
[21] Böttger, B., Apel, M., Santillana, B. and Eskin, D.G., Phase-field modelling of microstructure formation during the solidification of continuously cast low carbon and HSLA steels, IOP Conference Series: Materials Science and Engineering 33 (2012), pp. 12107.
[22] Allazadeh, M.R., Main Processes in Steel Production with continuously cast Method. (2015).
[23] Wolf, M. and Kurz, W., The effect of carbon content on solidification of steel in the continuous casting mold, MTB 12 (1981), 1, pp. 85–93.
[24] Mazumdar, S., & Ray, S. K., Solidification control in continuous casting of steel (2001), pp. 179–198.
[25] VOESTALPINE Industrieanlagenbau, GMBH, VAI Automation Secondary Cooling System (1998).
[26] Kou, S., and R. Mehrabian, Modeling and control of casting and welding processes.
[27] Liu, Y., Wang, W., Ma, F. and Zhang, H., Study of Solidification and Heat Transfer Behavior of Mold Flux Through Mold Flux Heat Transfer Simulator Technique: Part I. Development of the Technique, Metal and Material Trans B 46 (2015), 3, pp. 1419–1430.
[28] A. Maurya, P., Effect of casting speed on continuous casting of steel slab, International journal of Mechanical Engineering and Robotics Research, 2014.
[29] Wang, R., Bao, Y.-P., Li, Y.-H. and An, H.-H., Optimization of secondary cooling in continuous casting of round billet, Metall. Res. Technol. 112 (2015), 3, pp. 302.
[30] Bernhard, C., Die Stranggießforschung am Lehrstuhl für Metallurgie: Entwicklung, Status und Ausblick, Berg Huettenmaenn Monatsh 154 (2009), 1, pp. 20–26.
[31] Raudensky, M. and Horsky, J., Secondary cooling in continuous casting and Leidenfrost temperature effects, Ironmaking & Steelmaking 32 (2005), 2, pp. 159–164.
[32] Li, C., and Thomas, B.G., Thermomechanical finite-element model of shell behavior in continuous casting of steel, Metal and Materi Trans B 35 (2004), 6, pp. 1151–1172.
[33] Lee, J.E., Yeo, T.J., Hwan OH, K., Yoon, J.K. and Yoon, U.S., Prediction of cracks in continuously cast steel beam blank through fully coupled analysis of fluid flow, heat transfer, and deformation behavior of a solidifying shell, Metal and Mat Trans A 31 (2000), 1, pp. 225–237.
[34] Kozlowski, P.F., Thomas, B.G., Azzi, J.A. and Wang, H., Simple constitutive equations for steel at high temperature, Metal and Mat Trans A 23 (1992), 3, pp. 903–918.
[35] Li, G., Thomas, B.G. and Stubbins, J.F., Modeling creep and fatigue of copper alloys, Metall and Mat Trans A 31 (2000), 10, pp. 2491–2502.

[36] Maurya, A. and Jha, P., Effect of casting speed on continuous casting of steel slab, international journal of Mechanical Engineering and Robotics Research 1 (2014), pp. 13–21.
[37] Thomas, B.G., Samarasekera, I.V. and Brimacombe, J.K., Comparison of numerical modeling techniques for complex, two-dimensional, transient heat-conduction problems, MTB 15 (1984), 2, pp. 307–318.
[38] Ejær, H.G., and Mo, A., ALSPEN-A mathematical model for thermal stresses in direct chill casting of aluminum billets, MTB 21 (1990), 6, pp. 1049–1061.
[39] Brimacombe, J.K. and Sorimachi, K., Crack formation in the continuous casting of steel, MTB 8 (1977), 2, pp. 489–505.
[40] Analysis of thermal and mechanical behavior of high heat flux facing copper walls, 1996.
[41] Kelly, J.E., Michalek, K.P., O'connor, T.G., Thomas, B.G. and Dantzig, J.A., Initial development of thermal and stress fields in continuously cast steel billets, Metall and Mat Trans A 19 (1988), 10, pp. 2589–2602.
[42] Alizadeh, M., Edris, H., Shafyei, A., Mathematical modeling of Heat transfer of Steel Continuous Casting Process 3 (2006), 2, pp. 7–16.
[43] Rihan, Y.A., and Abd El-Bary, B., Computational Study of Heat Transfer and Solidification in Mold during the Continuous Casting of Steel, 2007.
[44] Sowa, L., and Bokota, A., Numerical Model of Thermal and Flow Phenomena the Process Growing of the CC Slab, Archives of Metallurgy and Materials 56 (2011), 2.
[45] Zhao, Y., Chen, D.F., Long, M.J., Shen, J.L. and Qin, R.S., Two-dimensional heat transfer model for secondary cooling of continuously cast beam blanks, Ironmaking & Steelmaking 41 (2014), 5, pp. 377–386.
[46] Andersson, J.O., Helander, T., Höglund, L., Shi, P. and Sundman, B., Thermo-Calc & DICTRA, computational tools for materials science, CALPHAD 26 (2002), 2, pp. 273–312.
[47] Mazumdar, D., A consideration about the concept of effective thermal conductivity in continuous casting, ISIJ Int. 29 (1989), 6, pp. 524–528.
[48] Hiester, H.R., Piggott, M.D., Farrell, P.E. and Allison, P.A., Assessment of spurious mixing in adaptive mesh simulations of the two-dimensional lock-exchange, Ocean Modelling 73 (2014), pp. 30–44.
[49] Zhang, W., Luo, S., Chen, Y., Wang, W. and Zhu, M., Numerical Simulation of Fluid Flow, Heat Transfer, Species Transfer, and Solidification in Billet Continuous Casting Mold with M-EMS, Metals 9 (2019), 1, pp. 66.
[50] Siddiqui, M.I.H. and Jha, P.K., Assessment of Turbulence Models for Prediction of Intermixed Amount with Free Surface Variation Using Coupled Level-Set Volume of Fluid Method, ISIJ Int. 54 (2014), 11, pp. 2578–2587.
[51] Yang, B., Deng, A., Li, Y., Xu, X. and Wang, E., Numerical simulation of flow and solidification in continuous casting process with mold electromagnetic stirring, J. Iron Steel Res. Int. 26 (2019), 3, pp. 219–229.
[52] Hardin, R.A., Liu, K., Kapoor, A., and Beckermann, C., A Transient Simulation and Dynamic Spray Cooling Control Model for Continuous Steel Casting.
[53] Ansys help, Fluent theory guide, Pull Velocity for Continuous Casting - 16.9 - Solidification and Melting, ANSYS 2022 R1,

https://ansyshelp.ansys.com/account/secured?returnurl=/Views/Secured/corp/v221/en/flu_th/flu_th_sec_melt_pull_velocity.html.
[54] Hannula, J., Porter, D.A., Kaijalainen, A. and Kömi, J., Evaluation of Mechanical Properties and Microstructures of Molybdenum and Niobium Micro alloyed Thermomechanically Rolled High-Strength Press Hardening Steel, JOM 71 (2019), 7, pp. 2405–2412.
[55] Szpunar, J.A., and Marder, A.R., The Effect of Alloy Content on Delayed Solidification in Stainless Steels, Acta Materialia 55 (2007), 3, pp. 1147–1159.
[56] Polmear, I. J., The Influence of Alloy Elements on Solidification Behavior in Stainless Steels, Physical Metallurgy of Metals and Alloys 5th (1998), pp. 253–275.